University of Nebraska - Lincoln

DigitalCommons@University of Nebraska - Lincoln

Theses, Dissertations, and Student Research from Electrical & Computer Engineering

Electrical & Computer Engineering, Department of

12-2016

Vector magneto-optical generalized ellipsometry for determining magneto-optical properties of thin films

Chad Briley
University of Nebraska-Lincoln, cbriley@engr.unl.edu

Follow this and additional works at: http://digitalcommons.unl.edu/elecengtheses

Part of the Electromagnetics and Photonics Commons

Vector magneto-optical generalized ellipsometry for determining magneto-optical properties of thin films

by

Chad Briley

A THESIS

Presented to the Faculty of

The Graduate College at the University of Nebraska

In Partial Fulfillment of Requirements

For the Degree of Master of Science

Major: Electrical Engineering

Under the Supervision of Professor Mathias Schubert

Lincoln, Nebraska

December 2016

Vector magneto-optical generalized ellipsometry for determining magneto-optical properties of thin films

Chad Michael Briley, M.S.

University of Nebraska, 2016

Advisor: Mathias Schubert

Modern growth techniques allow for highly complex nano scale thin films to be created. These new films possess highly anisotropic properties structurally, optically, and magnetically that are significantly different from that of their bulk counterparts and must be accurately characterized in order to optimize desired properties for applications in next generation devices. Current magnetometry techniques focus on high symmetry characterization, namely in and out of the sample plane, and therefore do not possess the capabilities to fully explore these anisotropic properties without complicated setups and multiple sample manipulations. The author describes a setup that combines generalized ellipsometry with an octu-pole vector magnet capable of producing magnetizing field of arbitrary amplitude and orientation to determine magneto-optical properties simultaneously in 3D without physical repositioning of samples. This combinatorial setup is referred to as vector magneto-optical generalized ellipsometry. Ferromagnetic thin films, both flat and three dimensionally structured, were probed via Mueller matrix ellipsometry at room temperature while under the influence of an external magnetic field. The resulting data was used to determine the magnetic induced changes in the dielectric tensor with model analysis and a differencing procedure. The determined changes in the dielectric tensor provide a 3D magnetic response and are used to determine magnetic anisotropy within nano-scale films both flat and highly anisotropic three dimensionally structured. The author presents and discusses results from the samples explored, both of which demonstrated shape induced magnetic anisotropy. In addition the author provides outlook for applications of the instrumentation and analysis procedure for future investigations.

Acknowledgements

There are so many people that helped me develop both in my research work and personally. I would like to start by thanking my adviser Dr. Mathias Schubert and for the opportunity to be involved with this incredible work group and the mentality of pushing the limits contained within. There have been countless times when the conversations held have helped my understanding, encouraged me, and have allowed me to see the bigger picture in general.

I would like to thank Dr. Eva Schubert for supporting my work financially and for giving insight and encouragement along the way.

I would also like to thank Dr. Ming Han for agreeing to be on my examining committee and lending his time and expertise. I would also like to thank him for teaching some of the most helpful and challenging classes I have participated in during my academic career.

I am thankful for the opportunity to work with Dr. Daniel Schmidt on the vector magneto-optical generalized ellipsometry project. Many long days were spent working under his supervision and side by side with him to bring the system to life.

Further, I would like to thank Dr. Tino Hofmann and Dr. Rafał Korlacki for the large amount of help they have provided throughout the course of my graduate and undergraduate career. They have always been there to help construct solutions to many of the problems encountered in this and many other projects as well as providing feedback for my proposed ideas.

I would like to thank my colleagues Dr. Philipp Kühne, Dr. Stefan Schöche, Dr. Keith B. Rodenhausen, Dr. Jennifer Gerasimov, Dr. Alex Boosalis, Dr. Dan Liang, Dr. Darin Peev, Alyssa Mock, Sean Knight, Ufuk Kilic, and Alex Ruder. They have all provided unique insight and a wonderful working environment that encourages development. They have truly made all of my experiences thus far quite remarkable and I am grateful for this.

I would like to especially thank Derek Sekora and Charles Rice who I have worked alongside in the classroom and lab since the first day of post-secondary education. Together we have helped each other out in our academic ventures and have watched ourselves grow.

Finally, I would like to thank my parents Mark and Jackie Briley and my sister Andrea Zurcher for supporting and encouraging me in my time at the University of Nebraska, I could not have achieved any of this without them.

List of Symbols and Acronyms

ALD: Atomic layer deposition

DDE: Dynamic data exchange

GLAD: Glancing angle deposition

GPIB: General purpose interface bus

HBLA: Homogeneous biaxial layer approach

L: Longitudinal

MO: Magneto-optical/magneto-optic

MOGE: Magneto-optical generalized ellipsometry

P: Polar

PVD: Physical vapor deposition

SCTF: Slanted columnar thin film

SE: Spectroscopic ellipsometry

SQUID: Superconducting quantum interference device

T: Transverse

TCP/IP: Transmission control protocol/internet protocol

VMOGE: Vector magneto-optical generalized ellipsometry

List of Figures

x

Contents

Chapter 1

Introduction

Magnetic materials have drawn curiosity from mankind for thousands of years. In modern technology magnetism and magnetic materials are present almost everywhere in many forms, from permanent magnets used in electric motors to the modern day collaboration of semiconductors and magnetic materials. There is still very much unknown about how magnetism can be engineered to take advantage of the nano scale properties, which are very much different from that of their bulk counterparts, that emerge from controlling the structure and crystallinity. [1, 2, 3, 4, 5, 6] New growth techniques and improvements in existing ones have supplied researchers the tools to have a high degree of control in thin films, to fabricate nanostructures as well as controlling film crystallinity and grain characteristics. Glancing angle deposition (GLAD) is an example of one of these growth processes within which nano structures can be grown from a variety of materials, [7, 8, 9, 10, 11, 12, 13] in a wide array of geometries [14, 15] and even as heterostructures. [16] With these advances in growth techniques, it is important to be able to accurately characterize thin film samples and the corresponding anisotropy of the structure and magnetism. Modern magnetometry techniques, including superconducting quantum interference (SQUID) and vibrating sample magnetometry (VSM), are capable of measuring only a few orientations with respect to the sample, primarily in-plane and out of plane magnetization. These techniques also require physical repositioning of the sample and lengthy calibrations to gain magnetic response measurements, as the device can only generate a magnetic field along one axis of the instrument coordinate system. To gain a better understanding of magnetically anisotropic samples it is important to utilize a measurement configuration that is capable of generating a magnetic field vector of arbitrary amplitude and orientation in 3D space, while simultaneously monitoring the resulting magnetic response of a sample in 3D. A setup that pairs generalized ellipsometry measurements with an octu-pole vector magnet referred to as vector magneto-optical

generalized ellipsometry (VMOGE) has been described. [17, 18, 19, 20]

Previous reports have investigated using the dielectric tensor to probe magnetic properties and have made calculations of observable quantities. [21, 22, 23, 24, 25] Further studies have investigated thin films for magneto-optical effects to observe magnetic anisotropy originating from crystallinity present and presented experimental results of such films. [26, 27, 28, 29, 30, 31] Three-dimensionally structured thin films of different compositions have been studied to determine magneto-optical properties including slanted columnar thin films (SCTF) films deposited by GLAD which will be investigated here. [32, 33, 8, 34, 35, 18, 19]

In this thesis the author will describe the work to develop the unique VMOGE process and outline the data acquisition procedure and subsequent analysis. The author will then demonstrate VMOGE results on a solid flat thin film and a SCTF sample both deposited from a ferromagnetic thin film. The presented work is organized as follows: Chapter 2 will contain the theoretical description of ellipsometry including the Jones and Mueller formalisms and the complete description of polarization in electromagnetic wave. The dielectric tensor will then be defined along with an appropriate optical model to determine it from data. The dielectric tensor will then be expanded to include magnetic-optic portions based on a connection with sample magnetization and electromagnetic waves. Finally, magneto-optical generalized ellipsometry data analysis will be described.

In Chapter 3 the VMOGE instrumentation will be described in two primary sections. First, the physical instrumentation is described as a combinatorial setup containing a commercial rotating analyzer ellipsometry system, a water cooled octu-pole vector magnet powered by four power supplies, and the goniometer on which the system is mounted. In the second section the author will describe the custom software that was created to calculate different magnetic hysteresis loop styles that are then coordinated and interfaced all of the components through measurement algorithms.

In Chapter 4 the author will present data on two different samples to demonstrate the robustness of this new and unique setup. The author will briefly describe the growth and characterization of the samples and the reason why these samples should be of interest for their expected magnetic anisotropies. The author will then discuss the results and compare the determined magneto-optical response with the expected magnetic response of a sample of the similar materials and geometry.

In Chapter 5 a summary of the work will be presented and future projects and application will be discussed.

Chapter 2

Spectroscopic Ellipsometry

Spectroscopic ellipsometry (SE) determines the relative change in the state of polarization of an electromagnetic plane wave upon interaction with a parallel planar sample, either by reflection or transmission, with respect to the polarization state of the incoming wave. Traditional SE measures a complex valued ratio (ρ) which can be expressed as two values (ψ, Δ), with ψ being the amplitude ratio and Δ being the phase difference of p- and s-polarized waves for electric field vectors parallel (p) and perpendicular (s) to the plane of incidence in a reflection setup. [36, 37] The ellipsometric parameters have the following form:

$$\rho = \left(\frac{E_p^{out}}{E_s^{out}} \right) / \left(\frac{E_p^{in}}{E_s^{in}} \right) = \tan\left(\Psi \right) e^{\mathrm{i}\Delta}. \tag{2.1}$$

If a sample exhibits anisotropic optical properties resulting in p and s mode conversion the ellipsometric parameters must be expanded to accurately describe the sample, by a generalized ellipsometry set of parameters.

2.1 Jones formalism

A complete mathematic description of completely polarized electromagnetic plane wave upon interaction with a non-depolarizing sample is provided by the Jones matrix. This connects an incoming Jones vector with an outward Jones vector by four complex-valued elements. The Jones vector contains two complex values corresponding to the field amplitude and phase of two orthogonal field components transverse to the direction of propagation. Generally these are denoted as as E_p and E_s, referring to respectively parallel and perpendicular electric fields as before. The Jones matrix is composed of Fresnel reflection coefficients and has the following form:
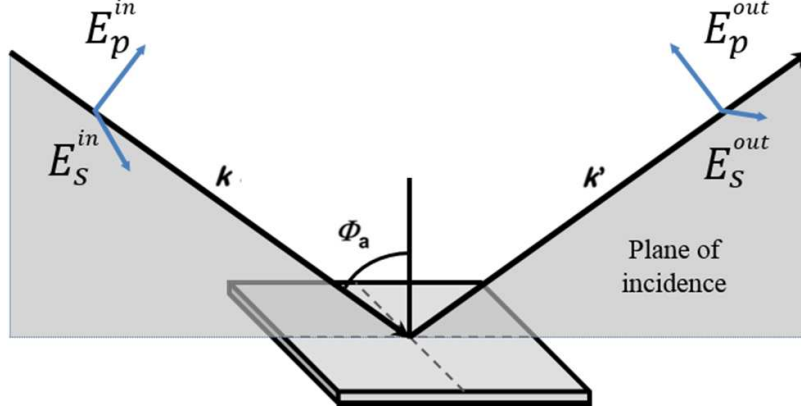
Figure 2.1: Definition of the ellipsometry setup with the incoming and outgoing wave vectors $\boldsymbol{k}$ and $\boldsymbol{k'}$, respectively, propagating at the angle (Φ_A) with respect to the sample normal, complex valued transverse electric fields parallel (E_p) and perpendicular (E_s) to the plane of incidence.

$$
\begin{bmatrix} E_p^{out} \\ E_s^{out} \end{bmatrix} = \boldsymbol{J} \begin{bmatrix} E_p^{in} \\ E_s^{in} \end{bmatrix} = \begin{bmatrix} r_{pp} & r_{ps} \\ r_{sp} & r_{pp} \end{bmatrix} \begin{bmatrix} E_p^{in} \\ E_s^{in} \end{bmatrix}. \tag{2.2}
$$

This formalism is able to describe multiple variations in polarized light from multiple optical elements by multiplying the individual transfer matrices together and is widely used in the field of ellipsometry but fails to take into account any plane waves that are not fully polarized or depolarizing samples, to account for this a more general presentation is required.

2.2   Mueller matrix formalism

The Stokes vector is composed of four real-valued components that completely describe the state of polarization of an electromagnetic wave including the degree of polarization. The Stokes vector is defined as follows:

$$
\begin{bmatrix} S_1 \\ S_2 \\ S_3 \\ S_4 \end{bmatrix} = \begin{bmatrix} I_p + I_s \\ I_p - I_s \\ I_{+45°} - I_{-45°} \\ I_{RHC} - I_{LHC} \end{bmatrix}, \tag{2.3}
$$

where I_p, I_s, $I_{\pm 45°}$, I_{RHC}, and I_{LHC} represent intensities for p, s, $\pm 45°$, right-hand circular, and left-hand circular polarized light respectively. The components of the Stokes vector can be mapped with three dimensional Cartesian coordinates onto the Poincaré sphere to provide a visualization of the complete state and degree of polarization. In this scheme the sphere is defined with the polar
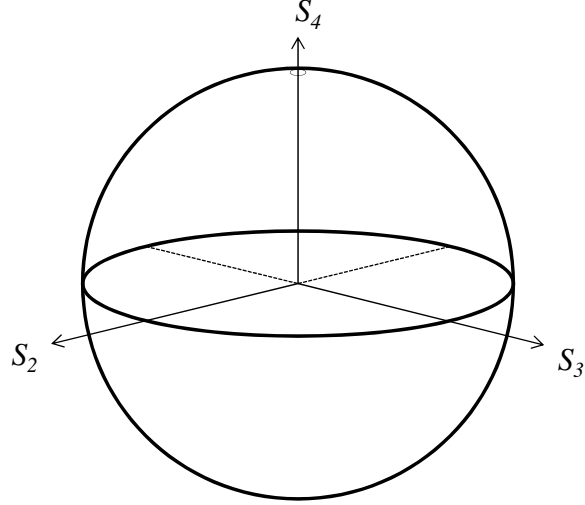
Figure 2.2: Poincaré sphere representation of polarization of electromagnetic waves.

axis as S_4 with parameters S_2 and S_3 defining an equatorial plane. The degree of polarization D_ρ can be determined by the Stokes vector via the following relation:

$$D_\rho = \frac{\sqrt{S_2^2 + S_3^2 + S_4^2}}{S_1}.$$ (2.4)

For a full mathematical description for electromagnetic plane waves interacting with a sample capable of depolarization, the Mueller matrix formalism provides the proper matrix. This 4x4 real valued matrix connects the incoming Stokes vector with an outgoing Stokes vector:

$$\begin{bmatrix} S_1 \\ S_2 \\ S_3 \\ S_4 \end{bmatrix} = \begin{bmatrix} M_{11} & M_{12} & M_{13} & M_{14} \\ M_{21} & M_{22} & M_{23} & M_{24} \\ M_{31} & M_{32} & M_{33} & M_{34} \\ M_{41} & M_{42} & M_{43} & M_{44} \end{bmatrix} \begin{bmatrix} S_1 \\ S_2 \\ S_3 \\ S_4 \end{bmatrix}.$$ (2.5)

Just as with the Jones matrix, a system of optical elements can have their corresponding Mueller matrix represented as the product of the individual matrices. [38]

$$\mathbf{M} = \prod_i \mathbf{M}_i.$$ (2.6)

This provides a systematic mathematical description that lends itself for designing and building optical instrumentation. With this, individual components of an optical system can be characterized independently and the resulting system with all of the components put together can be determined from the aforementioned individual characterizations.

2.3 Dielectric function tensor and anisotropy

When an electric field vector $\boldsymbol{E} = \boldsymbol{x}E_x + \boldsymbol{y}E_y + \boldsymbol{z}E_z$ is applied to a medium, charge separation and disturbance results, this polarization of the material is described the displacement vector $\boldsymbol{D} = \boldsymbol{x}D_x + \boldsymbol{y}D_y + \boldsymbol{z}D_z$. These two quantities are related to one another by the dielectric function ε to satisfy the equation $\boldsymbol{D} = \varepsilon\boldsymbol{E}$. More generally, to describe an anisotropic material the dielectric function tensor takes the form as follows:

$$\varepsilon = \begin{bmatrix} \varepsilon_{xx} & \varepsilon_{xy} & \varepsilon_{xz} \\ \varepsilon_{yx} & \varepsilon_{yy} & \varepsilon_{yz} \\ \varepsilon_{zx} & \varepsilon_{zy} & \varepsilon_{zz} \end{bmatrix}. \tag{2.7}$$

For a material with orthorhombic crystal symmetry the dielectric function tensor ε can be diagonalized through Euler rotations via a general tranformation matrix $\boldsymbol{A}$ possessing major palarizability axes $\boldsymbol{a}, \boldsymbol{b}, \boldsymbol{c}$ with the following form [36]:

$$\varepsilon = \boldsymbol{A}(\theta, \phi, \psi) \begin{bmatrix} \varepsilon_a & 0 & 0 \\ 0 & \varepsilon_b & 0 \\ 0 & 0 & \varepsilon_c \end{bmatrix} \boldsymbol{A}(\theta, \phi, \psi)^T, \tag{2.8}$$

$$\boldsymbol{A} = \begin{bmatrix} \cos(\psi)\cos(\phi) - \cos(\theta)\sin(\phi)\sin(\psi) & \cos(\psi)\cos(\phi) - \cos(\theta)\sin(\phi)\sin(\psi) & \sin(\theta)\sin(\phi) \\ \cos(\psi)\sin(\phi) + \cos(\theta)\cos(\phi)\sin(\psi) & -\sin(\psi)\sin(\phi) + \cos(\theta)\cos(\phi)\cos(\psi) & -\sin(\theta)\cos(\phi) \\ \sin(\theta)\sin(\psi) & \sin(\theta)\cos(\psi) & \cos(\theta) \end{bmatrix}. \tag{2.9}$$

2.4 Optical Modelling of Ellipsometric Data

To determine the dielectric function tensor ε, film thickness d, and other characteristics of a sample from measured ellipsometric data an optical model must be utilized. Optical models are constructed in a layered fashion with each layer of the model representing a layer in the thin film sample under analysis with a corresponding Mueller matrix or Jones matrix. These corresponding matrices for each layer will then follow a nested multiplication as presented with a product notation in Eq 2.6. Fitting algorithms are subsequently implemented in what is referred to as, best match model analysis, to determine appropriate values within each layer of the model to best match experimentally acquired data.

2.4.1 Homogeneous Biaxial Layer Approach

For anisotropic sample systems that possess birefringence a more complex approach must be taken when optically modelling. One such procedure that has been proven a successful in describing anisotropic thin films is what is know as the homogeneous biaxial layer approach (HBLA). [39] In the HBLA a generally anisotropic thin film layer that is homogeneous in all directions that is composed of one or more materials can be represented as a biaxial effective medium generally composed of a full anisotropic dielectric tensor and layer thickness. If the film possesses a symmetry that is at least orthorhombic the HBLA can be used to fit only the major polarizability axes of the diagonalized dielectric function tensor and corresponding rotation angles to minimize fitting parameters. This results in an effective dielectric tensor for a generally homogeneous biaxial thin film. For an SCTF sample the major polarizability axes will be aligned with the physical geometries of the nano columns.

2.5 Magneto-optics

2.5.1 Connecting magnetism and electromagnetic waves

Under the influence of an external magnetizing field $\boldsymbol{H}$, a magnetic sample can achieve a net spin polarization referred to as sample magnetization $\boldsymbol{M}$. These two fields added together are referred to as the induction magnetic field $\boldsymbol{B}$, the relation between these fields has the form

$$\boldsymbol{B} = \mu_0(\boldsymbol{H} + \boldsymbol{M}). \tag{2.10}$$

Upon interaction with an incident electric field vector $\boldsymbol{E}$ a magnetized sample will exhibit anisotropic optical properties proportional to the cross product between $\boldsymbol{M}$ and $\boldsymbol{E}$. In Cartesian coordinates, the diagonalized dielectric tensor ε of a magnetized material then exhibits anti-symmetric off-diagonal complex values $\varepsilon_{ij} = \mathrm{Re}\left\{\varepsilon_{ij}\right\} + \mathrm{i}\,\mathrm{Im}\left\{\varepsilon_{ij}\right\}\ (i,j=a,b,c)$. [22, 29, 40, 21] For small $\boldsymbol{H}$ these values are assumed here to be proportional to the sample magnetization $\boldsymbol{M} = (M_a, M_b, M_c)$ with a linear magneto-optical coupling parameter $\boldsymbol{Q} = (Q_a, Q_b, Q_c)$ that is assumed to be isotropic such that $Q_a \approx Q_b \approx Q_c$. The magneto-optical portion of ε can then be written as follows: [18]

$$\varepsilon^{\mathrm{MO}} = \begin{bmatrix} 0 & Q_c M_c(\boldsymbol{H}) & -Q_b M_b(\boldsymbol{H}) \\ -Q_c M_c(\boldsymbol{H}) & 0 & Q_a M_a(\boldsymbol{H}) \\ Q_b M_b(\boldsymbol{H}) & -Q_a M_a(\boldsymbol{H}) & 0 \end{bmatrix} = \begin{bmatrix} 0 & \varepsilon_{ab} & -\varepsilon_{ac} \\ -\varepsilon_{ab} & 0 & \varepsilon_{bc} \\ \varepsilon_{ac} & -\varepsilon_{bc} & 0 \end{bmatrix}. \tag{2.11}$$

The diagonalized dielectric tensor ε of a magnetized sample will be extended to include an off-diagonal anti-symmetric portion to account for magneto-optic effects. The new dielectric tensor of a magnetized sample will then have the general form:

$$\varepsilon = \varepsilon^{\mathrm{D}} + \varepsilon^{\mathrm{MO}} = \begin{bmatrix} \varepsilon_a & 0 & 0 \\ 0 & \varepsilon_b & 0 \\ 0 & 0 & \varepsilon_c \end{bmatrix} + \begin{bmatrix} 0 & \varepsilon_{ab} & -\varepsilon_{ac} \\ -\varepsilon_{ab} & 0 & \varepsilon_{bc} \\ \varepsilon_{ac} & -\varepsilon_{bc} & 0 \end{bmatrix}. \tag{2.12}$$

It can be observed that in this diagonalized presentation of the complete dielectric tensor of a magnetized sample it is possible to separate the magneto-optical portion from the non-magnetic portion through a differencing process.

2.5.2 Magneto-optical generalized ellipsometry

Magneto-optical generalized ellipsometry (MOGE) is a non-destructive magnetic characterization technique that uses the interaction of electromagnetic waves and sample magnetization, as previously described, to determine the change incurred in the dielectric tensor. Unlike other magnetic characterization processes, VSM and SQUID magnetometry for example, this process is beneficial as it can be performed on a sample of any size and will report values that reflect sample magnetization in 3D from a localized area.

In the MOGE process spectroscopic Mueller matrix data is first acquired from the sample under investigation without the presence of a magnetizing field to determine the thickness d and the full dielectric tensor ε through layered model analysis. Next, Mueller matrix data is acquired at select points during a magnetizing scan. These two data sets represent the field-free dielectric tensor $(\varepsilon^{\boldsymbol{B}=0})$ and the full dielectric tensor with magnetic field present $(\varepsilon^{\boldsymbol{B}\neq0})$. The two data sets are then differenced to isolate magneto-optical contributions to the measured Mueller matrix and the inherent underlying dielectric tensor of the sample with the following form:

$$\boldsymbol{M}^{MO} = \boldsymbol{M}_{\boldsymbol{B}\neq0} - \boldsymbol{M}_{\boldsymbol{B}=0}, \tag{2.13}$$

$$\varepsilon^{\mathrm{MO}} = \varepsilon^{\boldsymbol{B}\neq0} - \varepsilon^{\boldsymbol{B}=0} = \begin{bmatrix} \varepsilon_a & \varepsilon_{ab} & -\varepsilon_{ac} \\ -\varepsilon_{ab} & \varepsilon_b & \varepsilon_{bc} \\ \varepsilon_{ac} & -\varepsilon_{bc} & \varepsilon_c \end{bmatrix} - \begin{bmatrix} \varepsilon_a & 0 & 0 \\ 0 & \varepsilon_b & 0 \\ 0 & 0 & \varepsilon_c \end{bmatrix}. \tag{2.14}$$

To determine the changes incurred in the magneto-optical dielectric tensor a point-by-point fit is employed. This process does not make any magnetic-field dependent lineshape implementations in

the fitting, instead performs a best match model fit for three complex components $(\varepsilon_{ab}, \varepsilon_{ac},$ and $\varepsilon_{bc})$ assuming each to have an anti-symmetric counterpart such that $\varepsilon_{ij} = -\varepsilon_{ji}$ for each data point along the magnetizing scan. To visualize the MOGE data analysis procedure refer to the flowchart in Fig. (2.5.2)
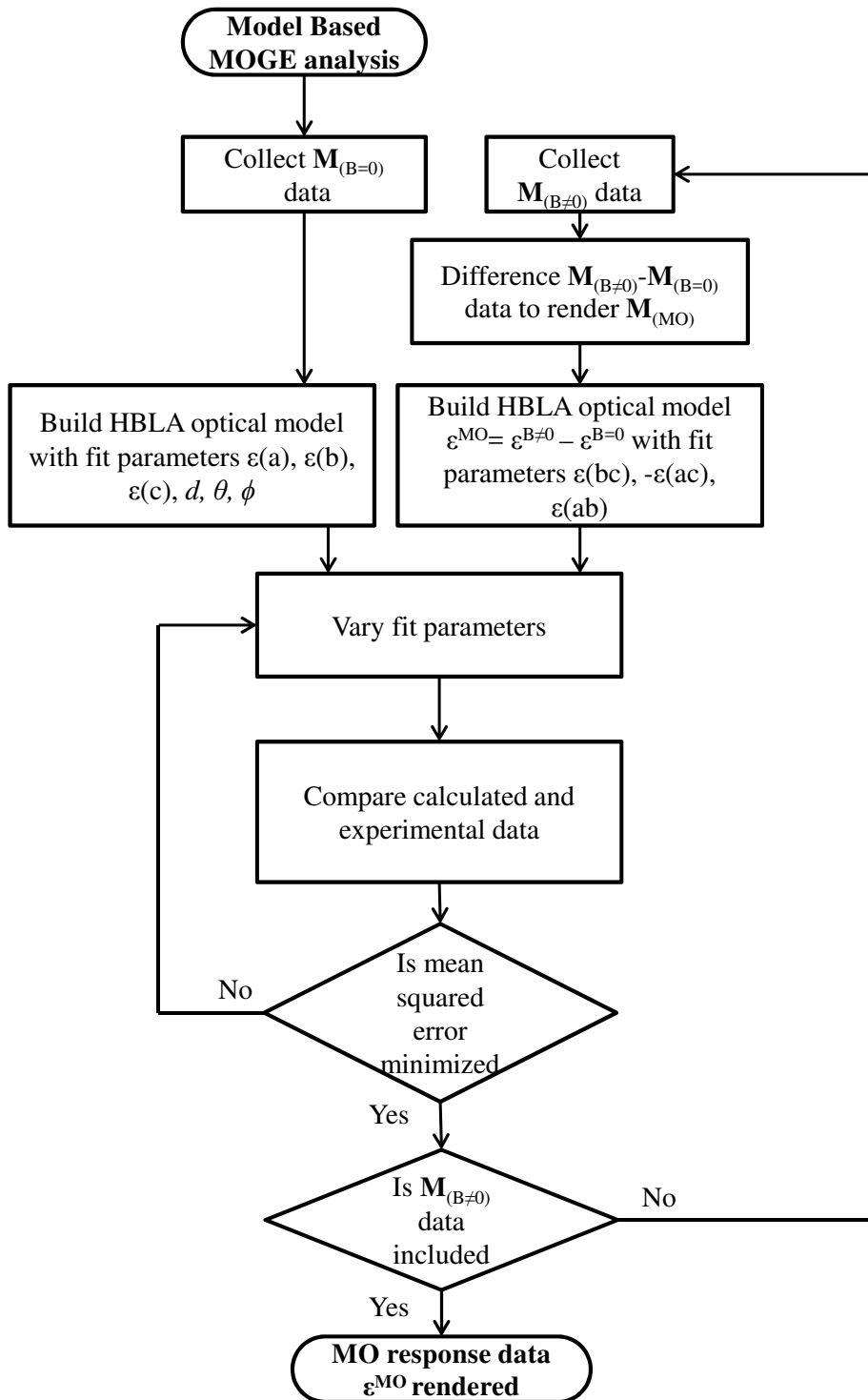
Figure 2.3: Flowchart depicting the general MOGE data analysis procedure and differencing process to render a MO response from a sample.

Chapter 3

Vector Magneto-Optic Generalized Ellipsometer

Extending MOGE measurements to highly anisotropic samples structurally, optically, and magnetically requires specialized instrumentation which is capable of generating magnetic field vectors with arbitrary orientation and amplitude in 3D vector space. This is necessary to probe unique magnetic axes of the sample system to isolate magnetic responses within the intrinsic coordinate system of the sample.

3.1   Physical setup

The VMOGE system consist of a custom built computer controlled octu-pole vector magnet Fig. (3.2) that is controlled by four independent power supplies. [41, 19, 20] Four magnetic coils pairs are positioned along the space diagonals of a cube and are wired in series, such that the magnetic field vectors from the pairs are oriented the same. This creates a homogeneous magnetizing field $\boldsymbol{H}$ at the center of the vector magnet where the sample is placed, as well as allowing for a beam path through which ellipsometric measurements can be performed. Custom machined water cooling plates are attached to the top and bottom of the magnet to dissipate heat from the coils and maintain a constant sample temperature during magnetic scans. The magnet can achieve a sustainable magnetic field up to $|\mu_0 \boldsymbol{H}| = 250$ mT. Samples are affixed to a glass sample holder that can be positioned and aligned with full 3D translation and tip-tilt with respect the sample plane. The vector magnet is mounted on the center of a goniometer that is carefully positioned such that the center of the magnet coordinate system is aligned with that of the ellipsometer system. On the arms of the goniometer a commercial rotating analyzer ellipsometer is mounted (V-VASE J.A. Woollam with Autoretarder) possessing a spectral range from

λ =300-1100 nm with the wavelengths selected by a monochromator capable of measuring 12 of the Mueller matrix elements consisting of the upper three rows of the Mueller matrix. The ellipsometer is equipped with focusing probes to confine the beam waist to approximately 1 mm such that the sample volume probed will be within a homogeneous magnetizing field of the vector magnet. With the addition of the focusing probes, the probe tips will be positioned physically within the vector magnet cage so care must be taken when changing angle of incidence in an automated measurement. The vertical posts on the housing of the coils can be repositioned to provide a large range of angles of incidence that can be accessed from $\Phi_A = 15° − 70°$, at $\Phi_A = 70°$ the probing beam will start to have substantial spread.

The coil pairs were individually calibrated with a commercial gaussmeter (Lakeshore 460 3-Channel Gaussmeter) that utilizes three orthogonal hall effect magnetic field sensors to measure the generated magnetic field to determine current to magnetic field conversion factors $\alpha_1, \alpha_2, \alpha_3, \alpha_4$ which were found to be constant for all coil pairs. To determine magnetic field spatial homogeneity of the vector magnet, the gaussmeter was translated through the center of the magnet with a high precision translation stage from all three coordinate axes x, y, z, the field was found to be symmetric in amplitude in all three directions. In Fig. (3.1) the experimentally determined spatial field homogeniety data can be observed. Notice that the field is symmetric and is above 99 percent field homogeniety for the central 1 mm^3 of the magnet where the sample surface is located.

3.2   Control program

To control the VMOGE system, a central control computer utilizing a LabVIEW program interfaces with the power supplies and an ellipsometer instrument control computer to coordinate ellipsometric data acquisition. The program contains three main blocks. The first block of the program initializes and reads in all inputs that will direct the file path and set the scan type, field amplitude, field resolution, and field orientation of the hysteresis magnetizing scan. The next block calculates the magnetic loops in 3D vector space and transforms them into current values for the power supplies which are stored in indexed data arrays. The final portion coordinates Mueller matrix ellipsometric scans with the power supplies to perform measurements at select field points along a hysteresis loop and saves the data. The latter two portions of the program will be investigated more thoroughly in the following section.
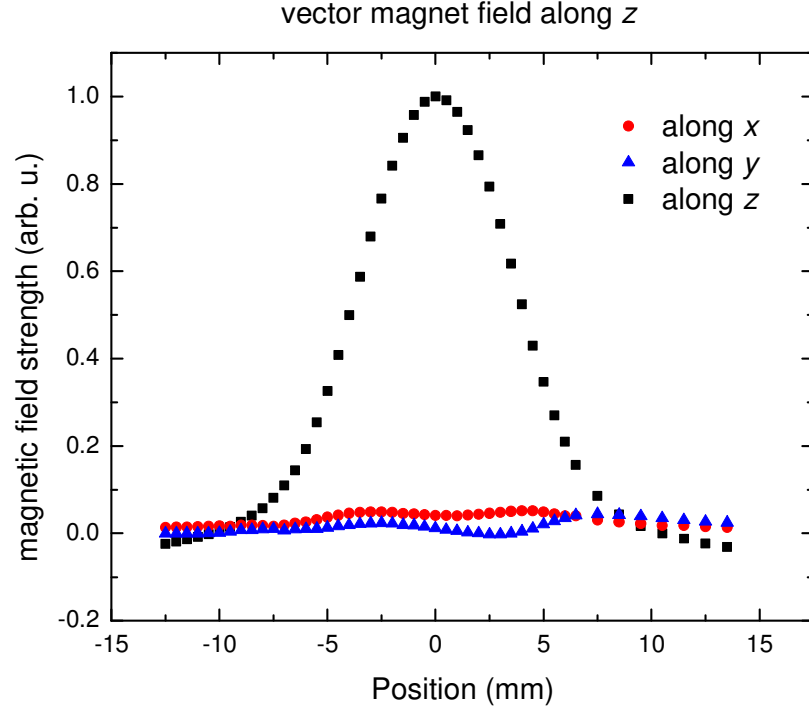
Figure 3.1: Normalized magnetic field homogeneity is plotted as a function of position from the center of the vector magnet.

3.2.1 Magnetic loop calculation

The current values to be sent to the power supplies for the magnetic hysteresis loop must be built as a 3 x n array with each column denoting the values for each magnetic field vector contained in the hysteresis loop. The hysteresis loop is determined by the user by parameterizing a closed loop in 3D vector space for the magnetic field. There are two main styles of magnetic hysteresis loops that are investigated, the directional hysteresis loop and the spatial hysteresis loop. Directional hysteresis magnetizing loops are field dependent loops that are fixed in a spatial direction. This is the type of magnetic hysteresis loop that is typically used as a standard magnetic characterization tool and is used to calculate magnetic coercivity H_c, saturation magnetization M_s, remanent magnetization M_r, and squareness of the demagnetization curve. In this setup the magnetic field is driven from an initial maximum value $\boldsymbol{H}_{max}$ and incrementally changed to the same maximum value but in the opposite direction $-\boldsymbol{H}_{max}$ and then back to the initial value $\boldsymbol{H}_{max}$ while maintaining a fixed spatial orientation. In a spatial magnetic hysteresis loop the magnetizing field is held at a constant value while the orientation is incrementally rotated through a complete circular loop. Three primary spatial hysteresis loops are defined as LT moving along the {xy}-plane starting oriented along the $+x$ axis and rotating towards the $+y$ axis, the TP follows
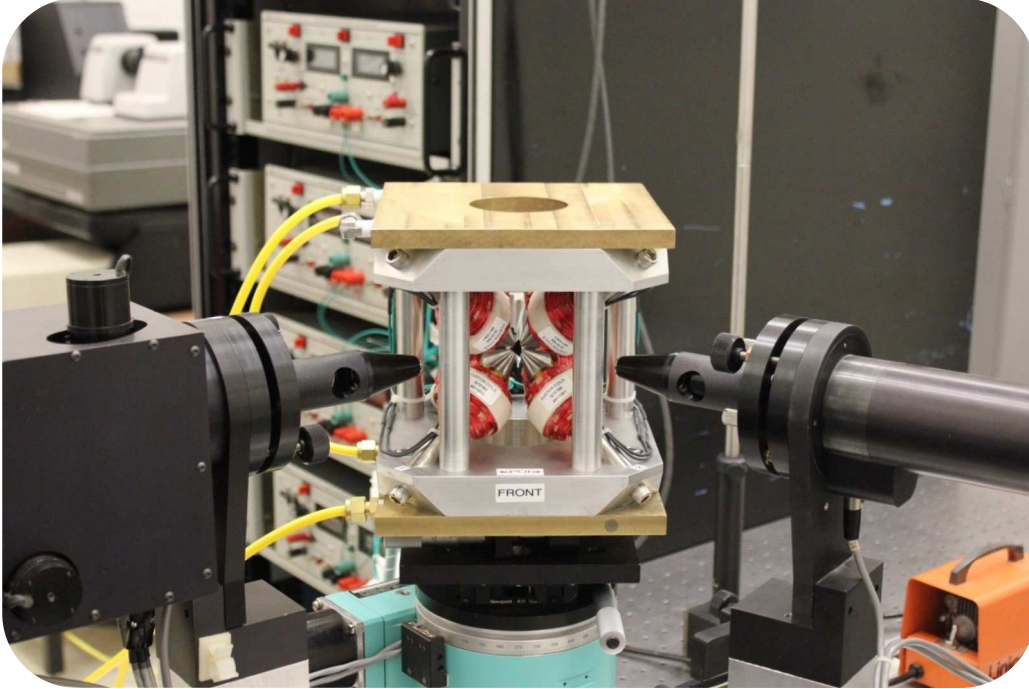
Figure 3.2: The vector magneto-optical system is pictured with the brass water-cooling plates on the top and bottom. The source and detector with focusing probes for the commercial ellipsometry system are seen on the sides and the control power supplies in the background.

the $\{yz\}$-plane starting along the $+y$ axis, and the PL follows the $\{zx\}$-plane starting along the $+z$ axis these planes are schematically depicted in Fig. (3.3). Both magnetic hysteresis loop styles can be arbitrarily oriented to match any anisotropy within a sample by applying the same rotation transformation discussed in section 2.3.

The 3D magnetization loop is put through a coordinate transformation to create four independent current values to be sent to the power supplies. Transforming each magnetic field vector into the overdetermined coil current system has an infinite amount of solutions, to overcome this a minimized norm solution is needed. This is achieved by utilizing a Moore-Penrose inverse matrix of the unit vectors of space diagonals of a cube [42] for the four independent coil pairs depicted in Fig. (3.2.1). This is multiplied with each magnetic field vector in the array to determine current values for each point in the loop. Having a minimized solution ensures minimized current values for each magnetic field vector and allows for monotonic current values throughout the loop. The determined current values are then multiplied by a linear scaling factor α that is empirically determined and relates the magnetic field that is measured in calibration to the current values passing through the coil pairs, as previously discussed. The equations describing this coordinate transformation appear as follows:
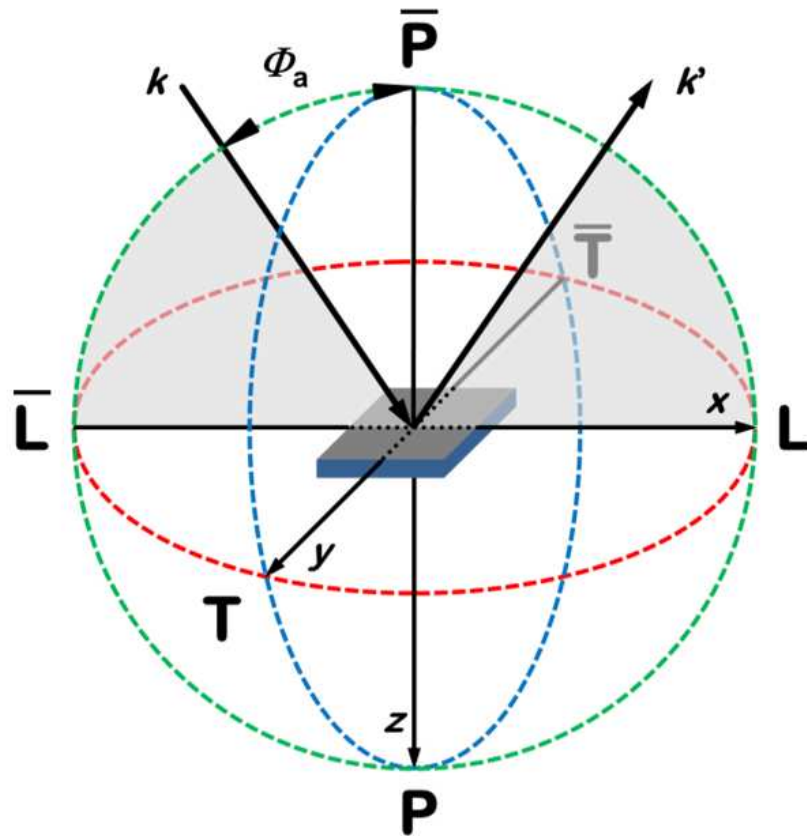
Figure 3.3: Displayed is the defined VMOGE Cartesian coordinate system x, y, z. The incident and reflected wave vectors are denoted $\boldsymbol{k}$ and $\boldsymbol{k'}$ respectively. Here the longitudinal, transverse, and polar Kerr geometries can be observed with respect to the laboratory coordinate frame.

$$\begin{bmatrix} H_x^L(t) \\ H_y^T(t) \\ H_z^P(t) \end{bmatrix} = C \begin{bmatrix} \alpha I_1(t) \\ \alpha I_2(t) \\ \alpha I_3(t) \\ \alpha I_4(t) \end{bmatrix}, \tag{3.1}$$

$$\text{Where } C = \begin{bmatrix} \hat{e}_{x1} & \hat{e}_{x2} & \hat{e}_{x3} & \hat{e}_{x4} \\ \hat{e}_{y1} & \hat{e}_{y2} & \hat{e}_{y3} & \hat{e}_{y4} \\ \hat{e}_{z1} & \hat{e}_{z2} & \hat{e}_{z3} & \hat{e}_{z4} \end{bmatrix} = \begin{bmatrix} -1 & +1 & +1 & -1 \\ +1 & +1 & +1 & +1 \\ -1 & -1 & +1 & +1 \end{bmatrix}, \tag{3.2}$$

$$\begin{bmatrix} \alpha I_1(t) \\ \alpha I_2(t) \\ \alpha I_3(t) \\ \alpha I_4(t) \end{bmatrix} = C^+ \begin{bmatrix} H_x^L(t) \\ H_y^T(t) \\ H_z^P(t) \end{bmatrix}. \tag{3.3}$$

3.2.2 Interfacing

The control computer is able to establish communication with the ellipsometer control computer through a transmission control protocol/internet protocol (TCP/IP) connection, subsequently data command strings that are sent from the LabVIEW control program are input and read out from WVASE ellipsometry software through a dynamic data exchange (DDE) link. The power supplies are sent control commands through a general purpose interface bus (GPIB) IEEE-288 standard connection by the LabVIEW control program. The LabVIEW control program will set up user defined measurement points along the loop, defining measurement resolution, by setting flags at appropriate field points. Once a measurement point in the magnetic loop is reached the set flag will commence a measurement subroutine. When the WVASE software responds that the measurement is completed, the acquired data is saved with a field point timestamp and the magnetic loop will continue to advance along with the measurement algorithm. A flow chart of the control program is depicted in Fig. (3.2.2).
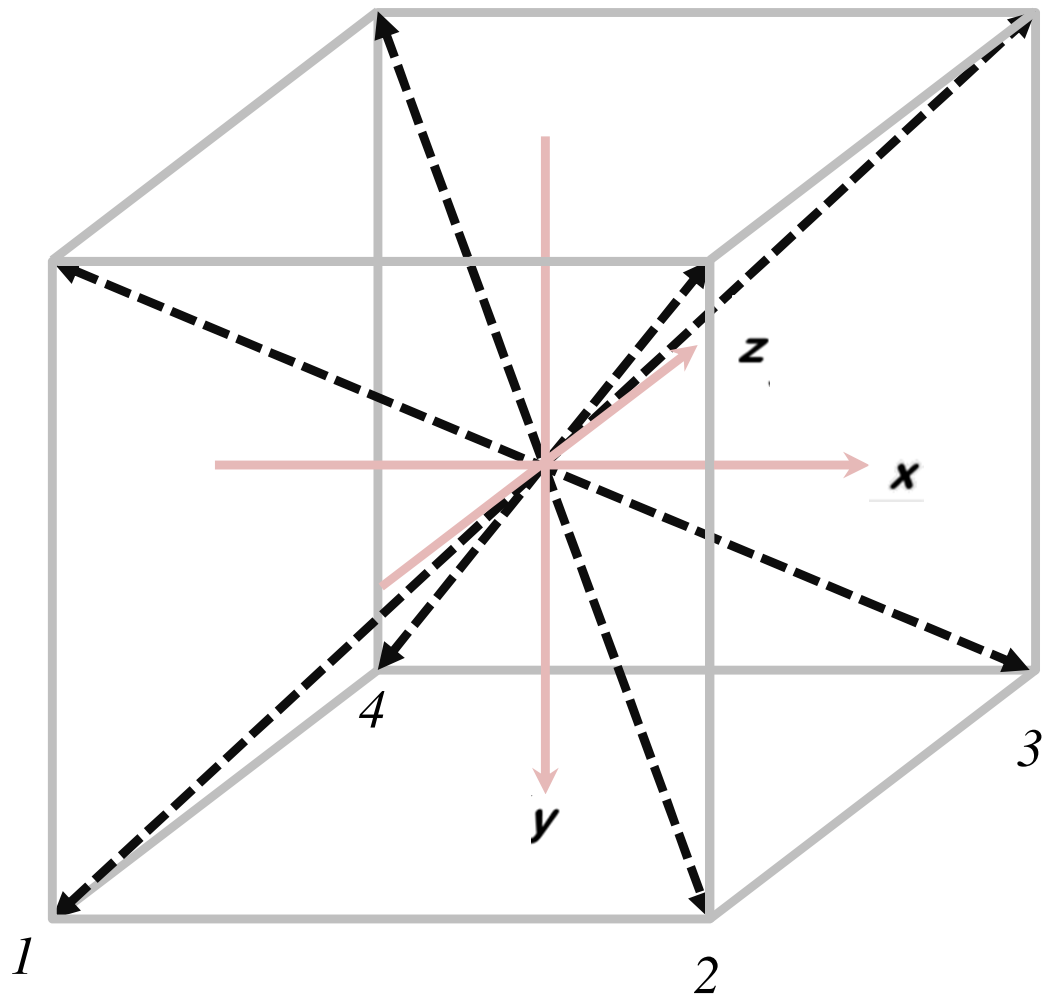
Figure 3.4: Schematic configuration showing the VMOGE coordinate system with respect to the coordinate system of the four magnet coil pairs used to calculate currents I_1, I_2, I_3, I_4 (dashed lines).
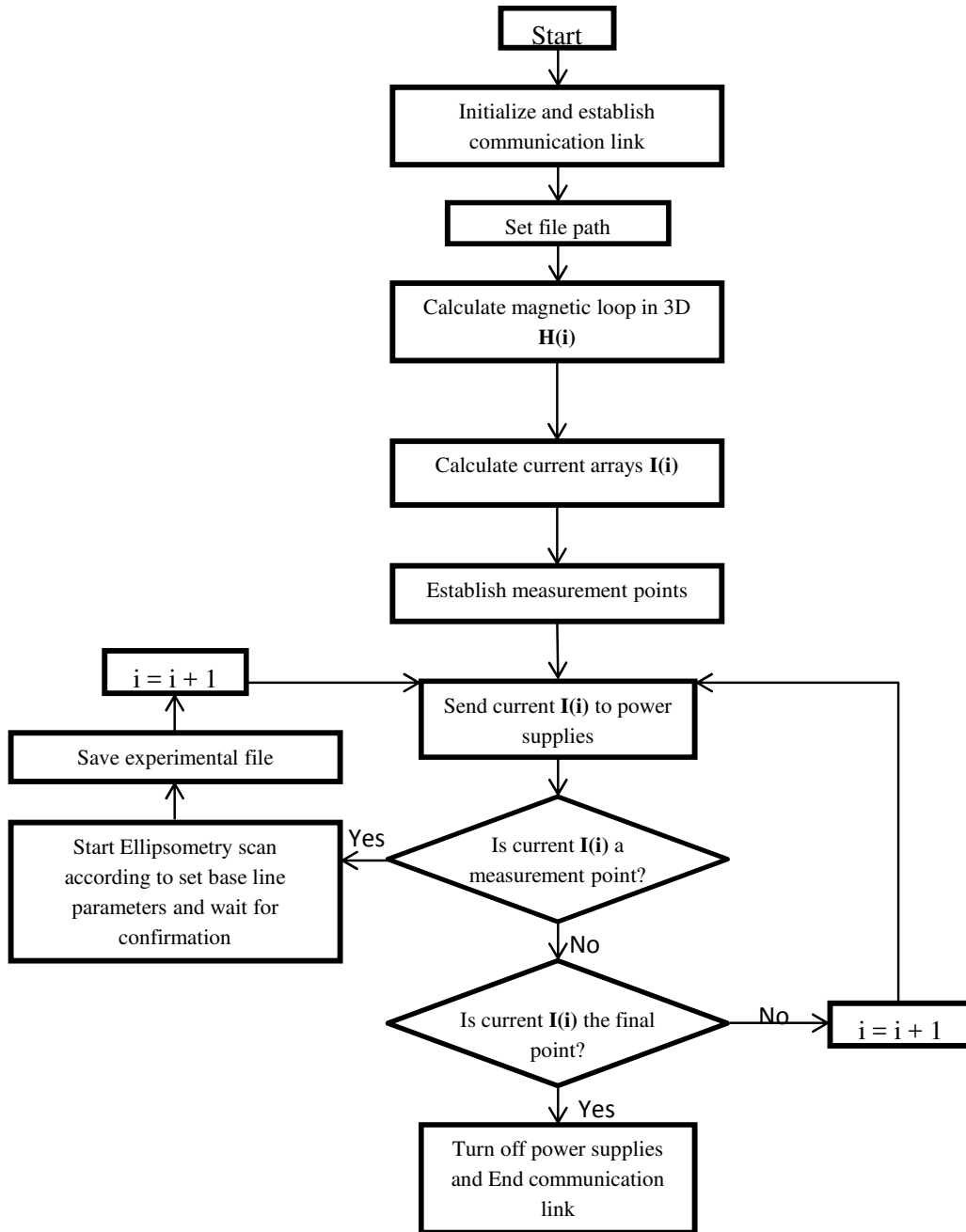
Figure 3.5: A flow chart of the LabVIEW control program for data acquisition.

Chapter 4

Magneto-optic response of thin films

4.1 Flat thin permalloy film

To initially explore the MO response of a sample, an isotropic ferromagnetic permalloy solid thin film was selected. This sample was deposited on a silicon (110) substrate with native oxide present under constant rotation by electron beam evaporation at normal incidence of $Ni_{80}Fe_{20}$ pellets (SCM Inc., Tallman, NY) in an ultra-high vacuum chamber. [19] The constant substrate rotation during deposition ensures a homogeneous growth of the resulting film of approximate thickness 100 nm. After deposition, the sample was immediately transferred to an atomic deposition layer (ALD) reactor (Fiji 200, CambridgeNanoTech Inc.). Approximately 3 nm of Al_2O_3 were conformally deposited by alternating cycles of trimethylaluminum and nanopure water at 70°C in a thermal deposition process. [19] The resulting alumina film passivates the permalloy film below it effectively preventing oxidation which would significantly change magnetic properties.

The sample was subsequently characterized by Mueller matrix ellipsometry using a $M2000^{\text{TM}}$, J. A. Woollam Co., Inc. instrument with rotation stage. Mueller matrix measurements determined the upper 12 components of the matrix from angles of incidence ($\Phi_A = 45°, 55°, 65°,$ and $75°$) from a single azimuthal orientation within the multi-wavelength range from 400 to 1400 nm. The data was analyzed with two isotropic material layers, one for the permalloy and the other for the Al_2O_3 passivation coating, to determine the full dielectric tensor (ε) of each layer of the film. This model was used as the baseline field-free optical model in MOGE data analysis.

Spatial hysteresis loops as previously described were utilized normal to and parallel to the sample plane. Point-by-point determined response to LT, PL, and TP-spatial hysteresis loops are

Figure 4.1: Point-by-point determined response in 3D of MO dielectric tensor components ε^{MO} from a solid flat thin permalloy film under the influence of a LT spatial hysteresis loop of field amplitude $\mu_0 \boldsymbol{H} = 170$ mT.

displayed in Figs. (4.1),(4.2), and (4.3). In Fig. (4.1) it can be observed that the response directly follows the external magnetizing field $\boldsymbol{H}_{x,y,z}$. In Fig. (4.2) and Fig. (4.3) the MO response to LP and TP-spatial hysteresis loops respectively demonstrate a similar response to each other but in orthogonal orientations. It is also important to note that the vertical axes in plots Fig. (4.2) and Fig. (4.3) have been expanded to show the slight canting present before the response flips in-plane orientation. The MO response to these out of plane loops show a preference to remain parallel to the sample surface until $\boldsymbol{H}_{x,y,z}$ passes the sample normal $\boldsymbol{H}_{0,0,z}$ at which point the MO response flips in-plane orientation. It is important to note that in this sample the intrinsic sample coordinate axes are aligned with the VMOGE coordinate system axes such that $(x, y, z) = (\boldsymbol{a}, \boldsymbol{b}, \boldsymbol{c})$. To demonstrate the in-plane magnetic properties an in-plane directional hysteresis scan with an initial field amplitude $\mu_0 \boldsymbol{H} = 100$ mT was performed with the externally applied magnetic field aligned in the L type configuration along the VMOGE x axis displayed in Fig. (4.4). It can be observed here that the in-plane coercivity is quite small $\mu_0 \boldsymbol{H}_c \approx 5$mT.

Figure 4.2: Point-by-point determined response in 3D of MO dielectric tensor components ε^{MO} from a solid flat thin permalloy film under the influence of a PL spatial hysteresis loop of field amplitude $\mu_0 \boldsymbol{H} =170$ mT.

Figure 4.3: Point-by-point determined response in 3D of MO dielectric tensor components ε^{MO} from a solid flat thin permalloy film under the influence of a TP spatial hysteresis loop of field amplitude $\mu_0 \boldsymbol{H} = 170$ mT.
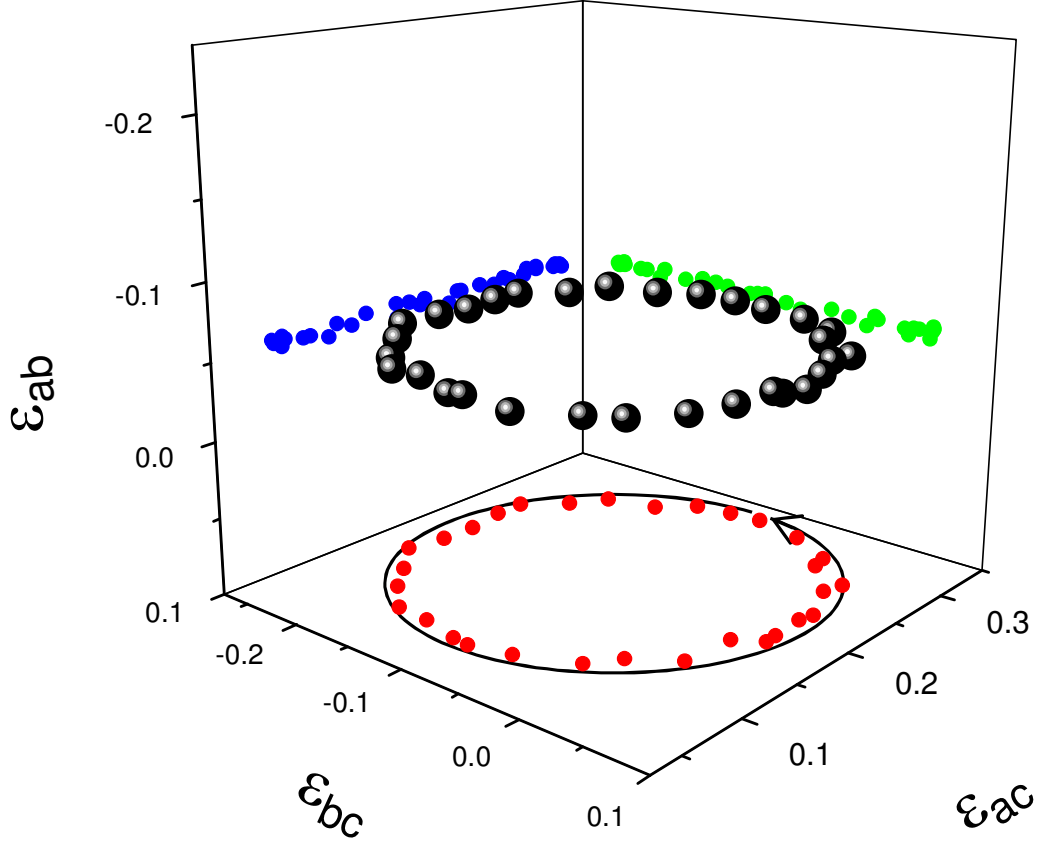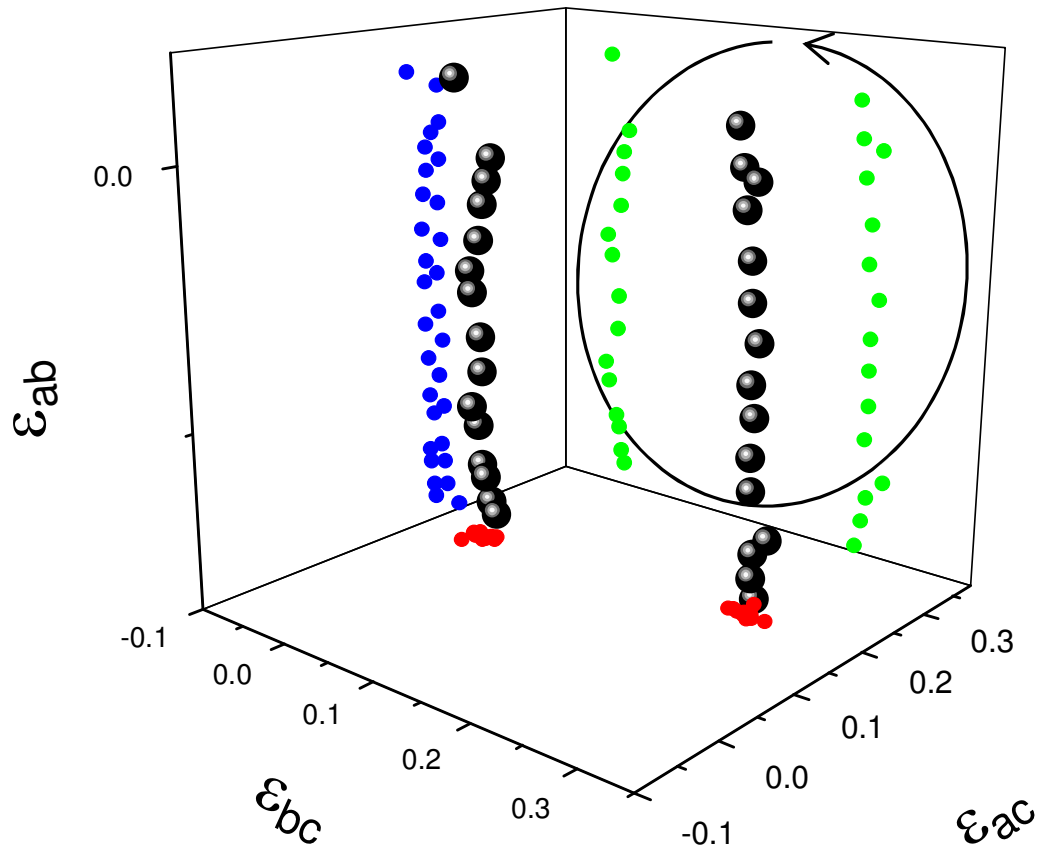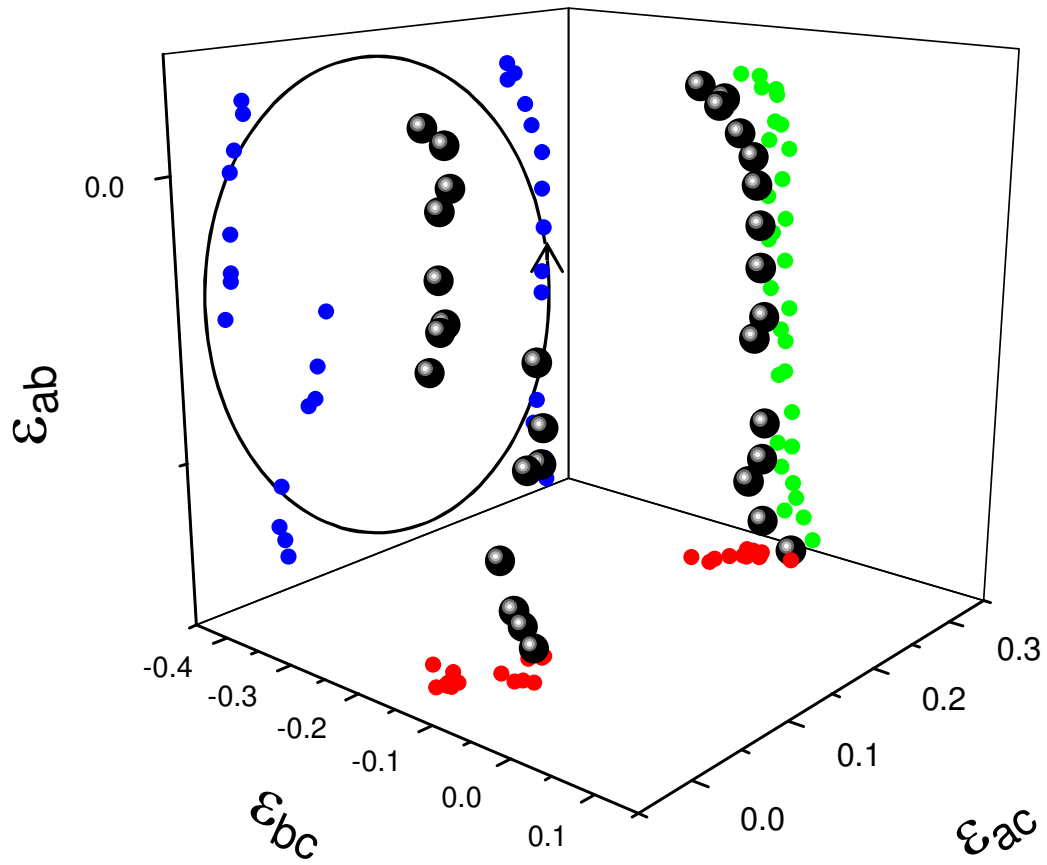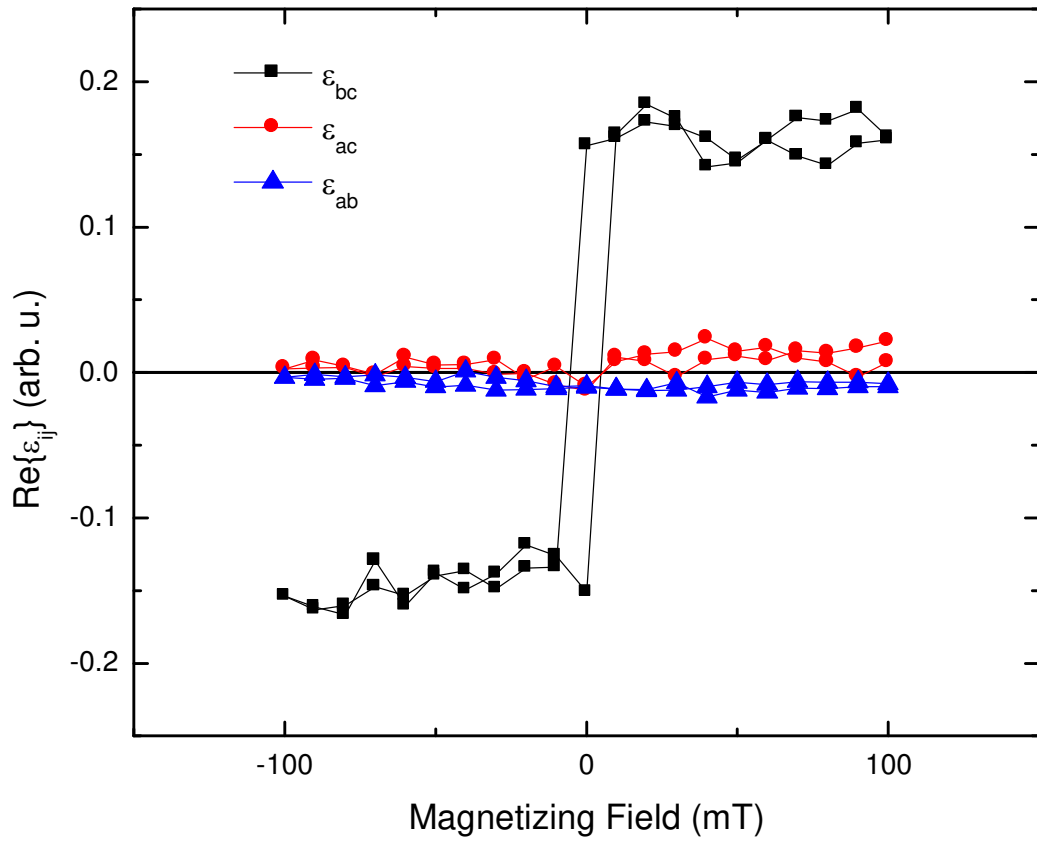
Figure 4.4: Point-by-point determined response of MO dielectric tensor components ε^{MO} from a solid flat thin permalloy film under the influence of a L type directional hysteresis scan of maximum field amplitude $\mu_0 \boldsymbol{H} = 100$ mT.

4.2   FeNi SCTF

The permalloy slanted columnar thin film (SCTF) sample was deposited on a similar substrate Si (110) in the same chamber via glancing angle deposition (GLAD) a physical vapor deposition process (PVD). In this process an electron beam thermally evaporates a target material, in this case permalloy, to create a particle flux. The sample was held at an oblique angle 85° to the particle flux so that a self shadowing process allows the film to grow in a coherent columnar fashion as seen if Fig. (4.5). After deposition the permalloy SCTF was immediately transferred to the ALD reactor for alumina passivation in the same fashion as the solid flat thin film sample. The resulting film as depicted in Fig. (4.5) is a permalloy SCTF and was initially analyzed with scanning electron microscopy (SEM)(Nova NanoSEM 450, FEI) to determine film thickness d, the inclination θ, and the column diameter. The thickness d was found to be approximately 100 nm with a columnar inclination angle of ($\theta \approx 65°$), and the columnar diameter is approximately 30 nm while the average length of the columns are approximately 230 nm.

The sample was optically characterized by Mueller matrix ellipsometry on a commercial ellipsometer ($M2000^{\text{TM}}$, J. A. Woollam Co., Inc.) with rotation stage. Mueller matrix measurements were performed from angles of incidence ($\Phi_A = 45°, 55°, 65°,$ and 75°) through a full azimuthal rotation of 360° by 6° increments and the resulting data was analyzed with an HBLA anisotropic layered optical model within which a single biaxial layer was used for the alumina coated SCTFs. The in-plane orientation φ denotes the azimuth between the plane of incidence and the projection of the nanocolumn axis onto the sample surface. The inclination angle θ is defined within the nanocolumn slanting plane between the nanocolumnar axis and the normal of the sample surface Fig. (4.5). The quantities φ and θ suffice to describe the orthogonal unit vectors parallel to the nanocolumn axis $\boldsymbol{N}_{\text{c}}$, parallel to the film surface $\boldsymbol{N}_{\text{a}}$, and perpendicular to the nanocolumn axis $\boldsymbol{N}_{\text{b}}$. The auxiliary system ($\boldsymbol{N}_{\text{a,b,c}}$) coincides with the major Cartesian dielectric polarizability axes of the nanocolumns, where a potentially existing, small monoclinic distortion is neglected here. [39] The resulting layer thickness determined from the HBLA was approximately 100 nm and the inclination angle determined was approximately $\theta = 64°$ which closely agrees with the SEM analysis.

To observe any magnetic anisotropy induced from the low dimensionality present in the SCTF with the VMOGE system, spatial hysteresis loops of field amplitude $|\mu_0\boldsymbol{H}| = 170 \ mT$ were carried out along the three principle planes of the VMOGE coordinate system LT, PL, and TP with the SCTF sample oriented with azimuthal angle $\varphi = 180°$. Fig. (4.6) depicts point-by-point
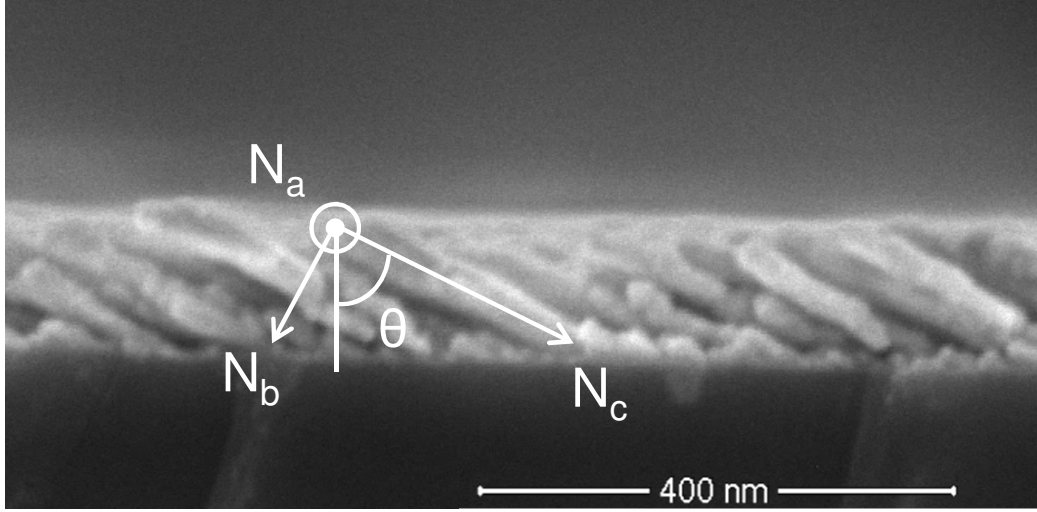
Figure 4.5: Cross section scanning electron micrograph of the alumina-passivated $Ni_{80}Fe_{20}$-SCTF sample investigated here. The SCTF thickness is about 100 nm and the diameter of the individual nanocolumns is approximately 30 nm. Overlaid is the auxiliary intrinsic coordinate system of the SCTF.

determined response in 3D of MO dielectric tensor components ε^{MO} within the intrinsic coordinate system of the SCTF ($\boldsymbol{N}_{a,b,c}$). It should be observed that all three of these spatial hysteresis loops will have non-zero projections of the external magnetizing field $\boldsymbol{H}$ onto the long axis of the SCTF and thus drives sample magnetism along this preferred direction. This can be seen as the large response in the dielectric tensor component ε_{ab} of the 3D plots that corresponds to the long the axis of the SCTF.

To gain understanding of characteristic magnetic properties, namely coercivity H_c and the squareness of the hysteresis loop, directional hysteresis magnetizing scans were performed. These directional hysteresis scans were performed with a maximum field amplitude of $\mu_0(H) = 250$ mT and the field was incremented in 25 mT steps between measurement points to define resolution of the hysteresis. Three types of directional hysteresis scans were performed on each sample orientation those being L, T, and P type configurations implying field orientations along the x, y, and z axes respectively. To observe the MO response with respect to sample orientation within the VMOGE system, three different sample orientations were selected $\varphi = 142°$, $180°$, and $219°$ these can be observed in Figs. (4.7), (4.8), and (4.9). It can be seen here that sample orientation $\phi = 180°$ is a high symmetry orientation such that the $\boldsymbol{N}_a$ axis of the sample can be isolated in a T type scan, while L and P scans will have external magnetizing field components projected onto SCTF intrinsic axes $\boldsymbol{N}_b$ and $\boldsymbol{N}_c$. Thus, through the VMOGE data analysis procedure 3D magnetic characteristic hysteresis curves can be determined for the three
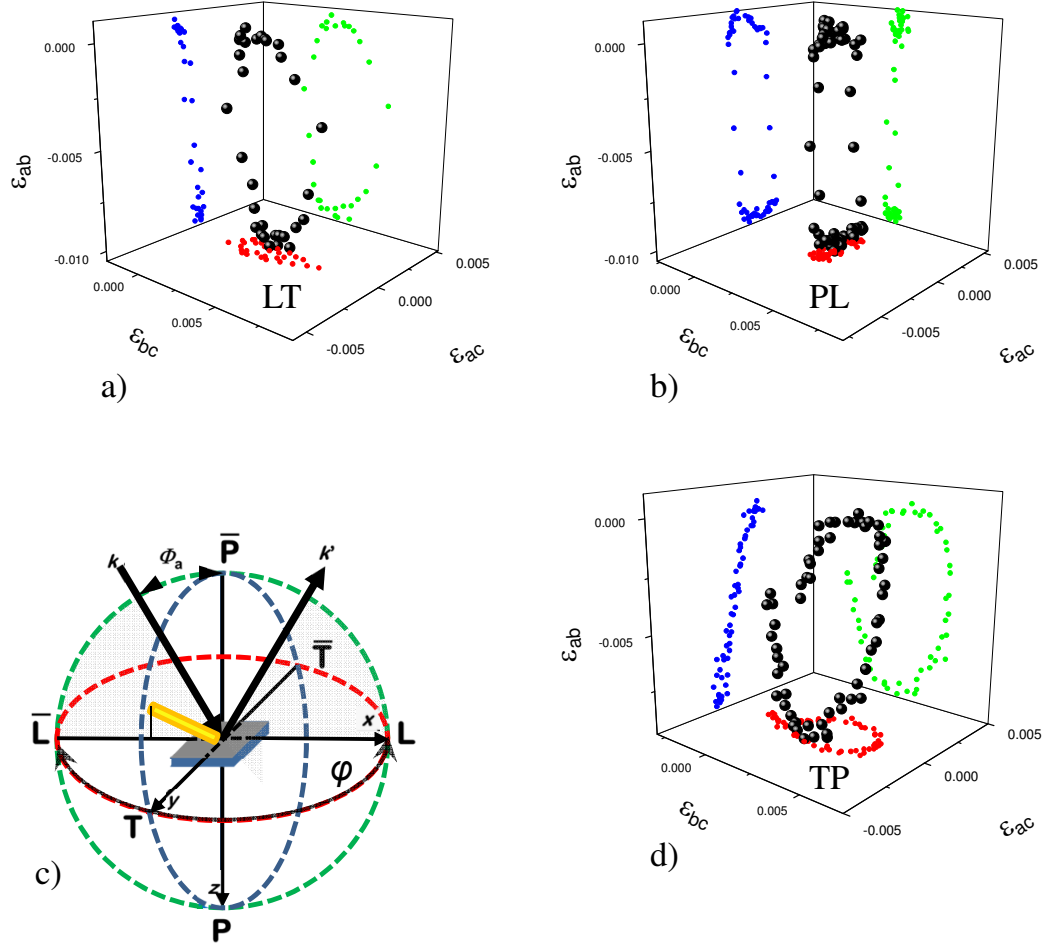
Figure 4.6: Point-by-point determined response plotted in 3D of MO dielectric tensor components ε^{MO} within the intrinsic coordinate system $\boldsymbol{N}_a, \boldsymbol{N}_b, \boldsymbol{N}_c$ from a permalloy SCTF film under the influence of an LT, PL, and TP spatial hystereses scans (a), (b), and (d) respectively with maximum field amplitude of $\mu_0 \boldsymbol{H}$ =170 mT. Schematic figure depicts the columnar orientation within the VMOGE coordinates system with respect to spatial hysteresis loops (c).

intrinsic axes for the structure. In sample orientations $\varphi = 219°$ and $142°$ the $\boldsymbol{N}_c$ axis of the SCTF sample will be oriented $+39°$ and $-38°$ from the plane of incidence. It follows that all intrinsic coordinate axes of the sample will have non-zero externally applied magnetizing field projections on them, thus driving magnetization along all intrinsic coordinate axes.

In Fig. (4.10) the MO response from an L type magnetizing scan on the SCTF sample in orientations $\varphi = 219°$ and $142°$ that have been transformed into the VMOGE coordinate system are depicted in Fig. (4.10)(a), (b), and (c) respectively. This representation gives a direct observation of the magnetic response of an SCTF in 3D. It can immediately be observed that the MO response will primarily follow the long axis of the column with a small amount of sample magnetization canting towards the direction of the applied field.
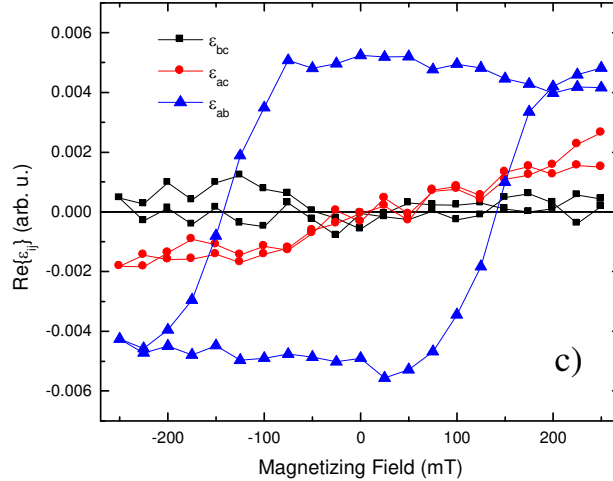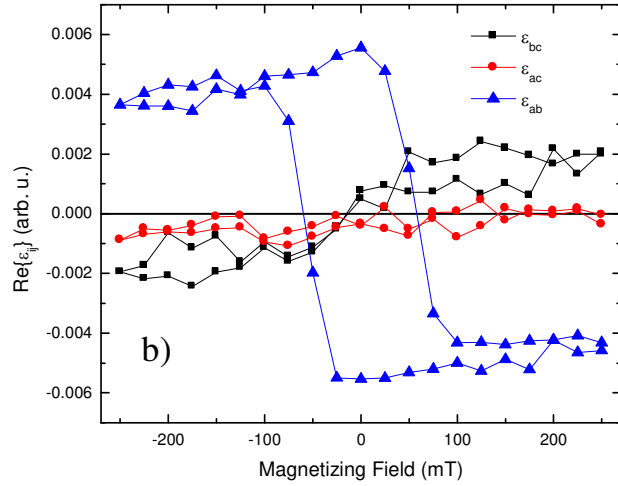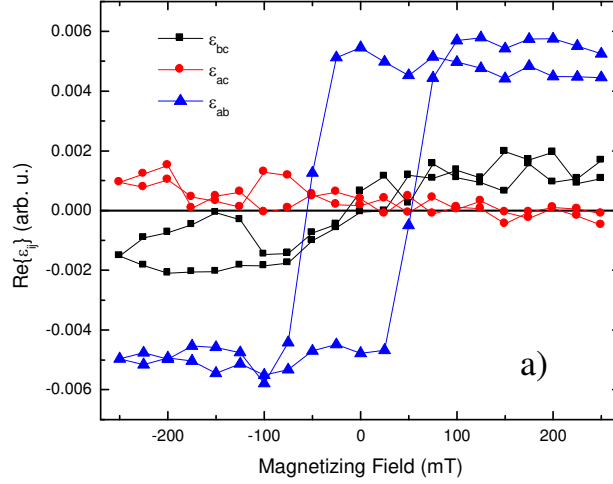
Figure 4.7: Point-by-point determined response plotted versus the magnitude of the externally applied magnetizing field of MO dielectric tensor components ε^{MO} within the intrinsic coordinate system $\boldsymbol{N}_a, \boldsymbol{N}_b, \boldsymbol{N}_c$ from a permalloy SCTF oriented with sample azimuth $\varphi = 142°$ film under the influence of an L, T, and P directional hystereses scans (a), (b), and (c) respectively with maximum field amplitude of $\mu_0 \boldsymbol{H} = 250$ mT.
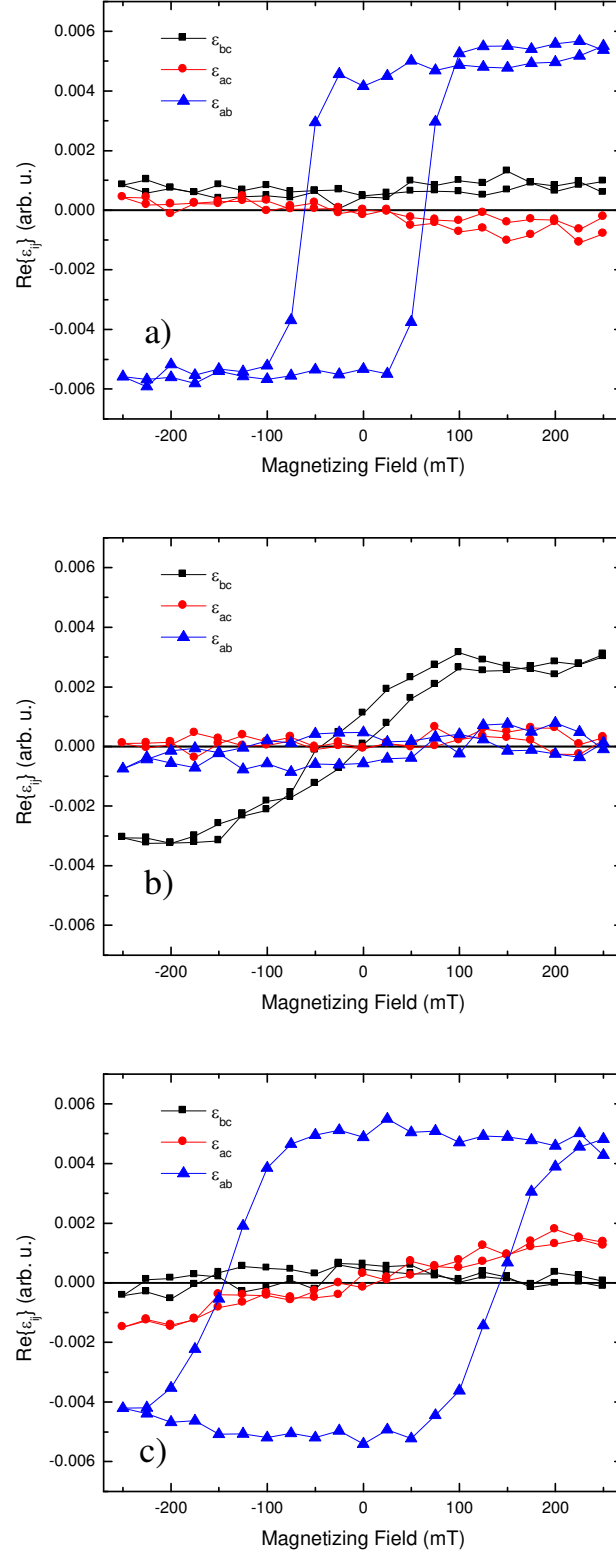
Figure 4.8: Point-by-point determined response plotted versus the magnitude of the externally applied magnetizing field of MO dielectric tensor components ε^{MO} within the intrinsic coordinate system $\boldsymbol{N}_a, \boldsymbol{N}_b, \boldsymbol{N}_c$ from a permalloy SCTF oriented with sample azimuth $\varphi = 180°$ film under the influence of an L, T, and P directional hystereses scans (a), (b), and (c) respectively with maximum field amplitude of $\mu_0 \boldsymbol{H} = 250$ mT.
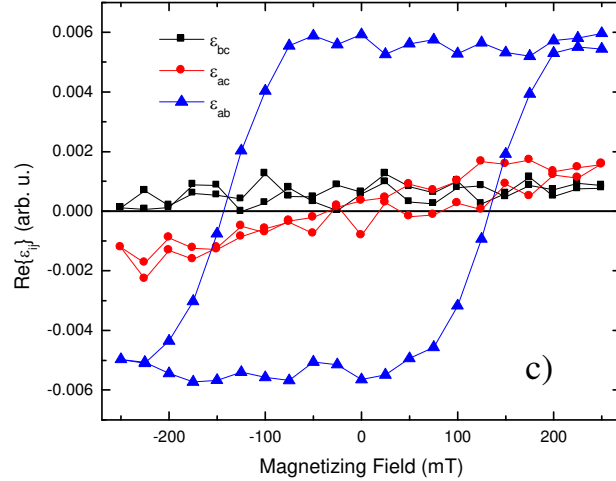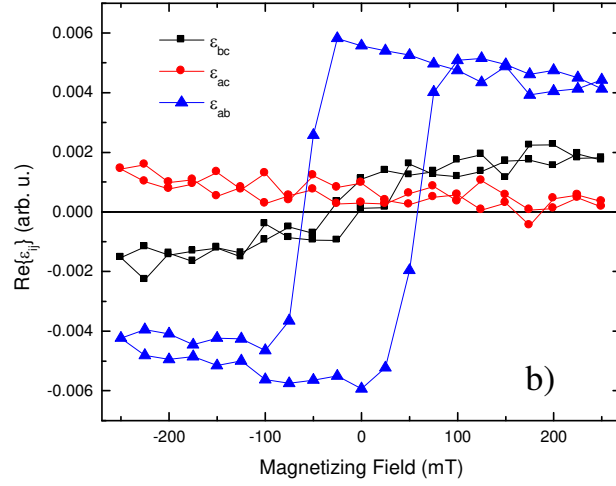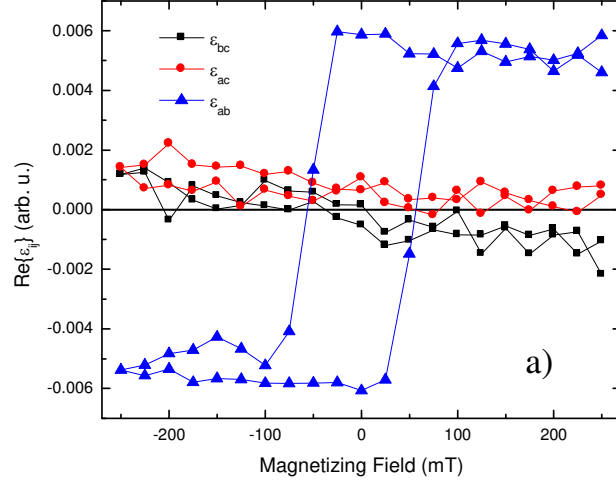
Figure 4.9: Point-by-point determined response plotted versus the magnitude of the externally applied magnetizing field of MO dielectric tensor components ε^{MO} within the intrinsic coordinate system $\boldsymbol{N}_a, \boldsymbol{N}_b, \boldsymbol{N}_c$ from a permalloy SCTF oriented with sample azimuth $\varphi = 219°$ film under the influence of an L, T, and P directional hystereses scans (a), (b), and (c) respectively with maximum field amplitude of $\mu_0 \boldsymbol{H} = 250$ mT.

Figure 4.10: Point-by-point determined response in 3D of MO dielectric tensor components ε^{MO} from a SCTF permalloy film transformed into the VMOGE coordinate system under the influence of a L type directional hysteresis scans of field amplitude $\mu_0 \boldsymbol{H} = 250$ mT.

4.3 Discussion

4.3.1 Flat thin film

Permalloy solid thin films such as this will exhibit a known in-plane anisotropy confining the preferred sample magnetization M direction to the sample plane t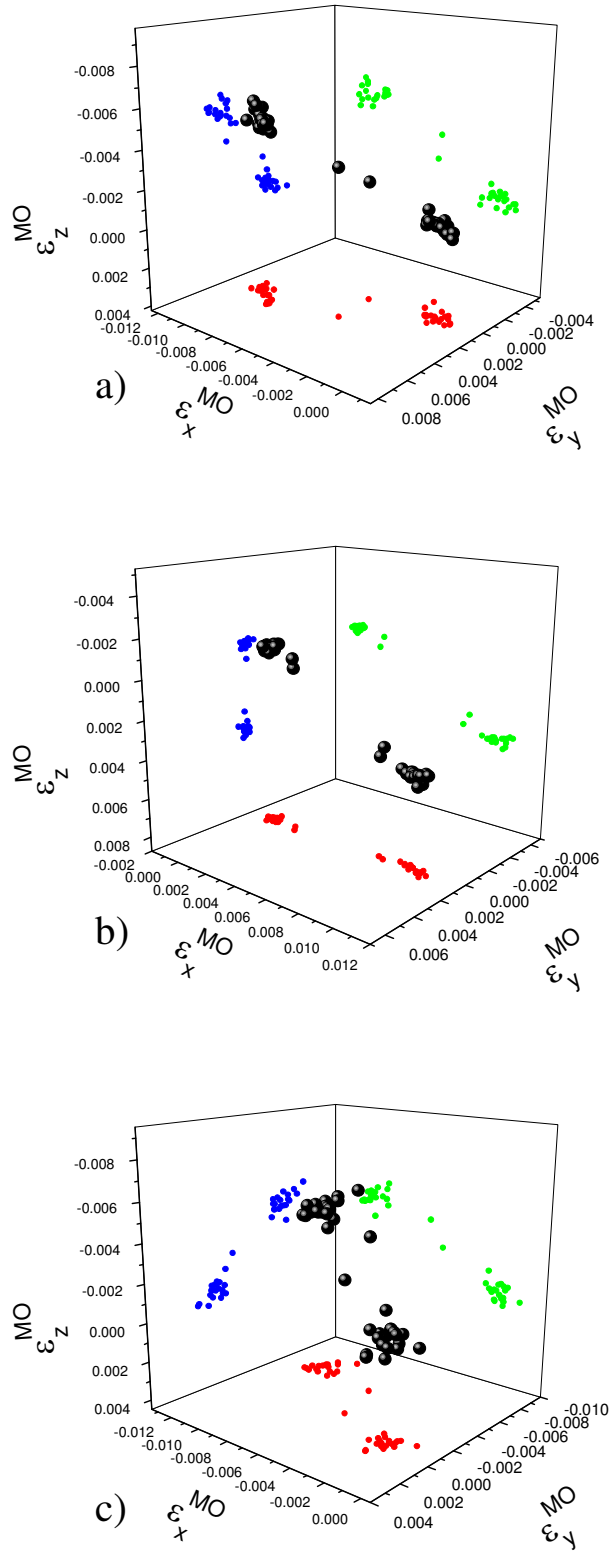hough no significant magnetic anisotropy will exist within the sample plane itself. [43, 44, 45] Spatial hysteresis loops were an ideal method to test this known magnetic response in the VMOGE system to demonstrate that the MO response is isotropic in-plane, as expected. This helps to confirm that the determined MO response of a thin film sample reflects the known magnetic response.

The VMOGE results from the solid flat thin permalloy film allow for immediate recognition of uniaxial anisotropy present in the film. The directional hysteresis scan performed on this sample subsequently allows one to immediately determine the magnetic characteristics including magnetic loop squareness and H_c within the plane of the film lending VMOGE as an extremely valuable tool for understanding magnetism in thin films.

4.3.2 Slanted columnar thin film

Permalloy SCTFs are a realization of a 1D coherent array and as such is expected exhibit shape induced magnetic anisotropy due to the internal demagnetization field. In a 1D magnetic material the demagnetization factor when assumed to be single domain will take the following form [43, 44, 6]:

$$H_c = \frac{2K_1}{\mu_0 M_s} + (1 - 3D) M_s, \tag{4.1}$$

where D is the demagnetization factor of the shape of the single domain magnetic particle with $D = 0$ for a cylinder of infinite aspect ratio. This will confine the preferred sample magnetization M direction parallel to the long axis of the individual nano-columns. Permalloy is known to have no significant magnetic anisotropy contribution due to any crystallographic magnetic anisotropy so all anisotropy observed from the sample will be from only shape induced anisotropy. In Figs. (4.7),(4.8), and (4.9) the rendered MO hysteresis loops allow for magnetic characterization of the SCTF within the intrinsic coordinate system of the structures. Here it can be seen that if the external magnetizing field is projected onto the long axis of the columns the magnetic coercivity can immediately be extracted and is approximately $H_c \approx 50$ mT which agrees with previous studies. [18, 46, 47, 48]

In Fig. (4.10) it can be seen that the VMOGE process is able to render the 3D MO response in the

experimental coordinate frame allowing for a direct 3D visualization of magnetic response to an externally applied field in highly anisotropic system. This demonstrates the robust nature and easily understood rendered data of the VMOGE system which will lend itself as an extremely important tool for 3D magnetic characterization.

Chapter 5

Summary and Outlook

In conclusion the author has illustrated the VMOGE instrumentation and data analyses process for determining the MO response of the dielectric tensor to monitor thin film sample magnetization under the influence of externally applied magnetic hysteresis scans. The VMOGE process is of special interest for investigating highly anisotropic samples, both magnetically and optically, by being able to orient the externally applied magnetizing field to unique axes of the sample while simultaneously monitoring the resulting response in 3D. The author described the initial vector magnet calibration process as well as the algorithm carried out in the custom control software that was made to calculate magnetic hysteresis scans, convert the magnetic field points to current values for the vector magnet, and coordinate ellipsometric measurements within the magnetic scans. Once the raw Mueller matrix data was acquired at select field points within the automated process, the author described the model analysis procedure to determine the MO portion of the dielectric tensor. To test the system and process the author selected two samples with well understood magnetic responses, one sample was a solid flat thin permalloy film with a preferential in-plane easy magnetic axis and the other sample was a permalloy SCTF that possessed shape induced anisotropy along the long axis of the columns. Finally, the author discussed determined MO response of each of these samples and the significance of the MO response matching the expected magnetic response.

There are limitless future studies of interest that can be performed with the now established VMOGE process. One primary avenue that could be explored would be to quantify the MO response with a 3D vectorized hysteresis response model for the sample sets investigated. This would provide a model that could be fit to the experimentally determined response to determine characteristic magnetic values such as the coercivity H_c and hysteresis loop squareness which and then compare with a measured response from a commercial magnetomer, such as SQUID. Another

experimental set of particular interest would be to perform studies on multi-layer heterogeneous SCTFs created via GLAD, composed of alternating magnetically hard and soft layers to realized theorized spring exchange systems. Systems such as this can achieve optimized magnetic energy products without the use of rare earth materials while retaining magnetism at high working temperatures.

References

[1] Ralph Skomski and J.M.D. Coey. Giant energy product in nanostructured two-phase magnets. *Phys. Rev. B*, 48(21):15812, 1993.

[2] Ralph Skomski and J.M.D. Coey. Nucleation field and energy product of aligned two-phase magnets-progress towards the1 mj/m 3'magnet. *IEEE Trans. Magn.*, 29(6):2860–2862, 1993.

[3] Ralph Skomski, G.C. Hadjipanayis, and David J. Sellmyer. Graded permanent magnets. *J. Appl. Phys.*, 105(7):07A733, 2009.

[4] Ralph Skomski, Yi Liu, J.E. Shield, G.C. Hadjipanayis, and David J Sellmyer. Permanent magnetism of dense-packed nanostructures. *J. Appl. Phys.*, 107(9):09A739, 2010.

[5] John J Croat, Jan F Herbst, Robert W Lee, and Frederick E Pinkerton. High-energy product nd-fe-b permanent magnets. *Appl. Phys. Lett.*, 44(1):148–149, 1984.

[6] D. Sellmyer and R. Skomski. *Advanced Magnetic Nanostructures*. Springer, 2006.

[7] D.O. Smith, M.S. Cohen, and G.P. Weiss. Oblique-incidence anisotropy in evaporated permalloy films. *J. Appl. Phys.*, 31(10):1755–1762, 1960.

[8] F. Tang, D.L. Liu, D.X. Ye, Y.P. Zhao, T.M. Lu, G.C. Wang, and A. Vijayaraghavan. Magnetic properties of co nanocolumns fabricated by oblique-angle deposition. *J. Appl. Phys.*, 93(7):4194–4200, 2003.

[9] F. Liu, M.T. Umlor, L. Shen, J. Weston, W. Eads, J.A. Barnard, and G.J. Mankey. The growth of nanoscale structured iron films by glancing angle deposition. *J. Appl. Phys.*, 85(8):5486–5488, 1999.

[10] Kevin Robbie and M.J. Brett. Sculptured thin films and glancing angle deposition: Growth mechanics and applications. *J. Vac. Sci. Techn. A*, 15(3):1460–1465, 1997.

[11] Daniel Schmidt, Tino Hofmann, Craig M Herzinger, Eva Schubert, and Mathias Schubert. Magneto-optical properties of cobalt slanted columnar thin films. *Appl. Phys. Lett.*, 96(9):091906–091906, 2010.

[12] L. Holland. The effect of vapor incidence on the structure of evaporated aluminum films. *J. Opt. Soc. Am.*, 43(5):376–380, 1953.

[13] D. Schmidt, B. Booso, T. Hofmann, E. Schubert, A. Sarangan, and M. Schubert. Generalized ellipsometry for monoclinic absorbing materials: determination of optical constants of cr columnar thin films. *Opt. Lett.*, 34(7):992–994, 2009.

[14] D. Schmidt, E. Schubert, and M. Schubert. Generalized ellipsometry determination of non-reciprocity in chiral silicon sculptured thin films. *Physica status Solidi (a)*, 205(4):748–751, 2008.

[15] Daniel Schmidt, Christian Müller, Tino Hofmann, Olle Inganäs, Hans Arwin, Eva Schubert, and Mathias Schubert. Optical properties of hybrid titanium chevron sculptured thin films coated with a semiconducting polymer. *Thin Solid Films*, 519(9):2645–2649, 2011.

[16] Yuping He and Yiping Zhao. Advanced multi-component nanostructures designed by dynamic shadowing growth. *Nanoscale*, 3(6):2361–2375, 2011.

[17] K. Mok, G. J. Kovács, J. McCord, L. Li, M. Helm, and H. Schmidt. Magneto-optical coupling in ferromagnetic thin films investigated by vector-magneto-optical generalized ellipsometry. *Phys. Rev. B*, 84:094413, Sep 2011.

[18] Chad Briley, Daniel Schmidt, Tino Hofmann, Eva Schubert, and Mathias Schubert. Anisotropic magneto-optical hysteresis of permalloy slanted columnar thin films determined by vector magneto-optical generalized ellipsometry. *Appl. Phys. Lett.*, 106(13):133104, 2015.

[19] Daniel Schmidt, Chad Briley, Eva Schubert, and Mathias Schubert. Vector magneto-optical generalized ellipsometry for sculptured thin films. *Appl. Phys. Lett.*, 102(12):123109–123109, 2013.

[20] Daniel Schmidt, Chad Briley, Eva Schubert, and Mathias Schubert. Vector magneto-optical generalized ellipsometry on passivated permalloy slanted columnar thin films. In *MRS Proceedings*, volume 1408. Cambridge Univ Press, 2012.

[21] Mathias Schubert, Thomas E Tiwald, and John A Woollam. Explicit solutions for the optical properties of arbitrary magneto-optic materials in generalized ellipsometry. *Appl. Opt.*, 38(1):177–187, 1999.

[22] Š Višňovský. Magneto-optical ellipsometry. *Czech J. Phys. B*, 36(5):625–650, 1986.

[23] P. Q. J. Nederpel and J. W. D. Martens. Magneto-optical ellipsometer. *Rev. Sci. Instr.*, 56(5):687–690, 1985.

[24] A. Berger and M.R. Pufall. Generalized magneto-optical ellipsometry. *Appl. Phys. Lett.*, 71(7):965–967, 1997.

[25] P. S. Pershan. Magneto-optical effects. *Journal of Applied Physics*, 38(3):1482–1490, 1967.

[26] G.S. Krinchik and V.A. Artemjev. Magneto-optic properties of nickel, iron, and cobalt. *J. Appl. Phys.*, 39(2):1276–1278, 1968.

[27] Timo Kuschel, Hauke Bardenhagen, Henrik Wilkens, Robin Schubert, Jaroslav Hamrle, Jaromír Pištora, and Joachim Wollschläger. Vectorial magnetometry using magnetooptic kerr effect including first-and second-order contributions for thin ferromagnetic films. *J. Phys. D: Appl. Phys.*, 44(26):265003, 2011.

[28] K. Postava, D. Hrabovský, O. Zivotský, J. Pištora, N. Dix, R. Muralidharan, J. M. Caicedo, F. Sanchez, and J. Fontcuberta. Magneto-optic material selectivity in self-assembled bifeo3-cofe2o4 biferroic nanostructures. *J. Appl. Phys.*, 105(7):–, 2009.

[29] Z.Q. Qiu and S.D. Bader. Surface magneto-optic kerr effect. *Rev. Sci. Instrum.*, 71(3):1243–1255, 2000.

[30] A. Berger and M.R. Pufall. Quantitative vector magnetometry using generalized magneto-optical ellipsometry. *J. Appl. Phys.*, 85(8):4583–4585, 1999.

[31] K. Mok, C. Scarlat, G.J. Kovács, L. Li, V. Zviagin, J. McCord, M. Helm, and H. Schmidt. Thickness independent magneto-optical coupling constant of nickel films in the visible spectral range. *J. Appl. Phys.*, 110(12):123110, 2011.

[32] M.T. Umlor. Uniaxial magnetic anisotropy in cobalt films induced by oblique deposition of an ultrathin cobalt underlayer. *Appl. Phys. Lett.*, 87(8):082505, 2005.

[33] F. Tang, D.L. Liu, D.X. Ye, T.M. Lu, and G.C. Wang. Asymmetry of magneto-optical kerr effect loops of co nano-columns grown by oblique incident angle deposition. *J. Magn. Magn. Mater.*, 283(1):65–70, 2004.

[34] Golda Hukic-Markosian, Yaxin Zhai, Danielle E. Montanari, Steven Ott, Adrianne Braun, Dali Sun, Zeev V. Vardeny, and Michael H. Bartl. Magnetic properties of periodically organized cobalt frameworks. *J. Appl. Phys.*, 116(1):013906, 2014.

[35] Juan Bautista González-Díaz, Antonio García-Martín, Gaspar Armelles, David Navas, Manuel Vázquez, Kornelius Nielsch, Ralf B. Wehrspohn, and Ulrich Gösele. Enhanced magneto-optics and size effects in ferromagnetic nanowire arrays. *Adv. Mat.*, 19(18):2643–2647, 2007.

[36] H. Fujiwara. *Spectroscopic Ellipsometry: Principles and Applications.* Wiley, 2007.

[37] R.M.A. Azzam and N.M. Bashara. *Ellipsometry and polarized light.* North-Holland personal library. North-Holland Pub. Co., 1977.

[38] Nathan Grieb Parke. Optical algebra. *Journal of Mathematics and Physics*, 28(1):131–139, 1949.

[39] Daniel Schmidt and Mathias Schubert. Anisotropic bruggeman effective medium approaches for slanted columnar thin films. *J. Appl. Phys.*, 114(8):083510, 2013.

[40] A.K. Zvezdin and V.A. Kotov. *Modern Magnetooptics and Magnetooptical Materials Materials.* Studies in condensed matter physics. Institute of Physics Pub., 1997.

[41] K. Mok, N. Du, and H. Schmidt. Vector-magneto-optical generalized ellipsometry. *Rev. Sci. Instrum.*, 82:033112, 2011.

[42] Roger Penrose. A generalized inverse for matrices. In *Mathematical proceedings of the Cambridge philosophical society*, volume 51, pages 406–413. Cambridge Univ Press, 1955.

[43] J.A. Osborn. Demagnetizing factors of the general ellipsoid. *Phys. Rev.*, 67(11-12):351, 1945.

[44] Charles Kittel. Theory of the structure of ferromagnetic domains in films and small particles. *Phys. Rev.*, 70(11-12):965, 1946.

[45] T.J. Silva, C.S. Lee, T.M. Crawford, and C.T. Rogers. Inductive measurement of ultrafast magnetization dynamics in thin-film permalloy. *J. Appl. Phys.*, 85(11):7849–7862, 1999.

[46] Samuel W. Yuan, H. Neal Bertram, Joseph F. Smyth, and Sheldon Schultz. Size effects of switching fields of thin permalloy particles. *IEEE Trans. Magn.*, 28(5):3171–3173, 1992.

[47] JF Smyth, S Schultz, DR Fredkin, DP Kern, SA Rishton, H Schmid, M Cali, and TR Koehler. Hysteresis in lithographic arrays of permalloy particles: Experiment and theory. *J. Appl. Phys.*, 69(8):5262–5266, 1991.

[48] M. Pardavi-Horvath, C.A. Ross, and R.D. McMichael. Shape effects in the ferromagnetic resonance of nanosize rectangular permalloy arrays. *IEEE Trans. Magn.*, 41(10):3601–3603, 2005.

Appendices

Publications, Conference Participation, and Awards

Publications

1. Vector Magneto-Optical Generalized Ellipsometry on Passivated Permalloy Slanted Columnar Thin Films, D. Schmidt, C. Briley, E. Schubert, and M. Schubert, Mat. Res. Soc. Symp. Proc. **1408**, BB15-19 (2012).

2. Vector Magneto-Optical Generalized Ellipsometry for Sculptured Thin Films, D. Schmidt, C. Briley, E. Schubert, and M. Schubert, Appl. Phys. Lett. **102**, 123109 (2013).

3. Anisotropic magneto-optical hysteresis of permalloy slanted columnar thin films determined by vector magneto-optical generalized ellipsometry, C. Briley, D. Schmidt, T. Hofmann, E. Schubert, and M. Schubert, Appl. Phys. Lett. **106**, 133104 (2015)

4. Effects of annealing and conformal alumina passivation on anisotropy and hysteresis of magneto-optical properties of cobalt slanted columnar thin films, C. Briley, A. Mock, R. Korlacki, T. Hofmann, E. Schubert, and M. Schubert, Appl. Surf. Sci. , (2016).

5. Optical and structural properties of cobalt-permalloy slanted columnar heterostructure thin films, D. Sekora, C. Briley, M. Schubert, and E. Schubert, Appl. Surf. Sci. , (2016).

6. Generalized ellipsometry critical point analysis from the far infrared to the deep ultra violet for single crystalline beta (gallia) Ga_2O_3, A. Mock, R. Korlacki, C. Briley, V. Darakchieva, E. Janzen, B. Monemar, Y. Kumagai, M. Higashiwaki, E. Schubert, and M. Schubert, Phys. Rev. B , (2016).

Conferences

1. Vector Magneto-Optical Generalized Ellipsometry on Sculptured Thin Films with Forward Calculated Uniaxial Response Simulation, C. Briley, T. Hofmann, D. Schmidt, E. Schubert,

and M. Schubert AVS 61st International Symposium and Exhibition (AVS-61), Baltimoe, MA, November (2014).

2. Anisotropic Magneo-Optical Hysteresis of Permalloy Slanted Columnar Thin Films Determined by Vector Magneto-Optical Generalized Ellipsometry, C. Briley, D. Schmidt, T. Hofmann, E. Schubert, and M. Schubert, WSE-9, Twente, Netherlands, February (2015).

3. Vector magneto-optical generalized ellipsometry on heat treated sculptured think films: A study of the effects of Al_2O_3 passivation coatings on magneto-optical properties, C. Briley, A. Mock, D. Schmidt, T. Hofmann, E. Schubert, and M. Schubert, AVS 62nd International Symposium and Exhibition (AVS-62), San Jose, CA, October (2015)

4. Vector magneto-optical generalized ellipsometry on nanostructured magnetic thin films of complex anisotropy C. Briley, A. Mock, R. Korlacki, T. Hofmann, E. Schubert, R. Skomski, and M. Schubert, ICSE-7, Berlin, Germany, June (2016).

Awards

1. Second place award, Anisotropic Plasmon Resonances in Nanostructured Thin Films: An Optical Model Approach, C. Briley, D. Sekora, T. Hofmann, E. Schubert, and M. Schubert, UNL Graduate Research Fair, Lincoln, NE, April (2015).

2. Spectroscopic Ellipsometry Topical Focus Session Student award winner, Vector Magneto-Optical Generalized Ellipsometry on Sculptured Thin Films with Forward Calculated Uniaxial Response Simulation, C. Briley, T. Hofmann, D. Schmidt, E. Schubert, and M. Schubert, AVS 61st International Symposium and Exhibition (AVS-61), Baltimoe, MA, November (2014).

3. Second place award, Vector Magneto-optical generalized ellipsometry, C. Briley, D. Schmidt, T. Hofmann, E. Schubert, M. Schubert, UNL Graduate Research Fair, Lincoln, NE, April (2013).